MM1.5: METHODS, ANALYSIS & INSIGHTS FROM MULTIMODAL LLM FINE-TUNING

Haotian Zhang°, **Mingfei Gao**°, **Zhe Gan**°, **Philipp Dufter**⋆, **Nina Wenzel**⋆, **Forrest Huang**⋆, **Dhruti Shah**⋆, **Xianzhi Du**⋆, **Bowen Zhang**⋆, **Yanghao Li**⋆, **Sam Dodge**, **Keen You**, **Zhen Yang**, **Aleksei Timofeev**, **Mingze Xu**, **Hong-You Chen**, **Jean-Philippe Fauconnier**, **Zhengfeng Lai**, **Haoxuan You**, **Zirui Wang**, **Afshin Dehghan**, **Peter Grasch**⋆, **Yinfei Yang**†
Apple
{haotian.zhang2,mgao22,zhe.gan,yinfeiy}@apple.com
°First authors; ⋆Core authors; †Project lead

ABSTRACT

We present **MM1.5**, a new family of multimodal large language models (MLLMs) designed to enhance capabilities in text-rich image understanding, visual referring and grounding, and multi-image reasoning. Building upon the MM1 architecture, MM1.5 adopts a data-centric approach to model training, systematically exploring the impact of diverse data mixtures across the entire model training lifecycle. This includes high-quality OCR data and synthetic captions for continual pre-training, as well as an optimized visual instruction-tuning data mixture for supervised fine-tuning. Our models range from 1B to 30B parameters, encompassing both dense and mixture-of-experts (MoE) variants, and demonstrate that careful data curation and training strategies can yield strong performance even at small scales (1B and 3B).[1] Through extensive empirical studies and ablations, we provide detailed insights into the training processes and decisions that inform our final designs, offering valuable guidance for future research in MLLM development.

1 INTRODUCTION

Multimodal Large Language Models (MLLMs) have emerged as an increasingly active research topic in recent years. Closed-source models, such as GPT-4o (Islam & Moushi, 2024), GPT-4V (OpenAI, 2024), Gemini-1.5 (Team et al., 2023; Reid et al., 2024), and Claude-3.5 (Anthropic, 2023), have demonstrated remarkable capabilities in advanced multimodal understanding. Meanwhile, open-source models, such as the LLaVA series of work (Liu et al., 2023b;a; 2024a; Li et al., 2024c), InternVL2 (Chen et al., 2024b), Cambrian-1 (Tong et al., 2024a) and Qwen2-VL (Bai et al., 2023; team, 2024), are rapidly narrowing the performance gap. There has also been growing interest in developing models capable of understanding single-image, multi-image, and video data using a single set of model weights (Li et al., 2024c). Further discussion of recent works is in Appendix A.1.

Building upon MM1 (McKinzie et al., 2024), we introduce MM1.5, a new family of MLLMs carefully designed to enhance a set of core capabilities. Specifically, we focus on the following aspects.

- **OCR.** MM1.5 supports arbitrary image aspect ratios and resolutions of up to 4 Megapixels. By incorporating carefully selected OCR data to enhance text comprehension across different training stages, MM1.5 excels at understanding text-rich images.
- **Visual referring and grounding.** MM1.5 offers robust, fine-grained image understanding, extending beyond text prompts to interpret *visual* prompts such as points and bounding boxes. Moreover, MM1.5 can generate grounded responses by grounding text output with image bounding boxes. This capability is notably under-explored in most open-source models (*e.g.*, LLaVA-OneVision (Li et al., 2024c) and Phi-3-Vision (Abdin et al., 2024b)), and even in strong proprietary models like GPT-4o, which rely on set-of-mark (SoM) prompting (Yang et al., 2023) to reference image regions.

[1] Additionally, we introduce two specialized variants: MM1.5-Video, designed for video understanding, and MM1.5-UI, tailored for mobile UI understanding, detailed in Appendix A.7 and A.8 correspondingly.

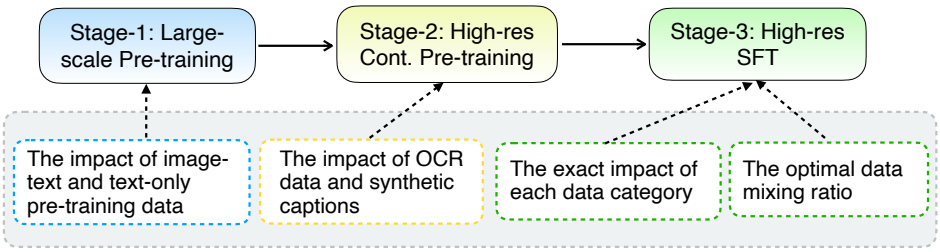

Figure 1: Recipe for building MM1.5. Model training contains three stages: (i) large-scale pre-training with low-resolution images (378×378), (ii) continual pre-training with high-resolution (up to 4 Megapixels) OCR data and synthetic captions, and (iii) supervised fine-tuning (SFT). At each stage, we aim to identify the optimal data mix and assess the impact of each data type.

- **Multi-image reasoning.** MM1.5 benefits from large-scale interleaved pre-training, resulting in strong in-context learning and multi-image reasoning capabilities right out of the box. We further improve its capabilities via supervised fine-tuning (SFT) on additional multi-image data.

Our primary focus is on the most efficient model scales, 1B and 3B, together with their corresponding Mixture-of-Experts (MoE) variants, and demonstrates that even relatively small MLLMs can achieve competitive performance on various downstream tasks. Furthermore, we demonstrate that the MM1.5 recipe exhibits strong scaling behavior all the way to 30B parameters, achieving competitive performance across a wide range of benchmarks.

Building performant MLLMs is a highly empirical endeavor. While the overarching goal and the high-level training procedure are well-defined, the finer details of their execution remain unclear. In developing MM1.5, we choose to retain the same model architecture as MM1 (McKinzie et al., 2024), enabling us to focus on refining and investigating the intricacies of our data-centric training recipes. Our attention is centered on the following key aspects:

- **Continual Pre-training.** We introduce an additional high-resolution continual pre-training stage preceding the SFT stage, which we found crucial for boosting text-rich image understanding performance. We ablate the impact of two kinds of data: (i) text-rich OCR data, focusing on detailed transcription of text within images; and (ii) high-quality synthetic image captions.
- **SFT.** While considerable prior work discusses SFT data for MLLMs, there is still limited exploration into how each category of SFT data can affect the final model's performance. In particular, the impact of data supporting each capability on other capabilities is understudied. We conduct extensive ablations to identify trade-offs and synergies, ultimately constructing a mixture from public datasets that contributes to well-balanced performance across a wide set of capabilities.
- **Dynamic High-resolution.** Furthermore, for *high-resolution* image encoding, we follow the popular any-resolution approach, dynamically dividing the image into sub-images (Li et al., 2023i; Zhang et al., 2024b), and conduct thorough ablations to refine key details in our design.

Unlike most open-source models focusing solely on SFT (Liu et al., 2023b;a; 2024a), MM1 demonstrated strong zero-shot and few-shot learning capabilities through large-scale pre-training. In developing MM1.5, we aim to retain these strengths and more effectively transfer them to the SFT stage. To achieve this, We further extend MM1's pre-training by exploring the impact of text-only data and optimizing the ratio of different pre-training data types. This approach improves performance on knowledge-intensive benchmarks and enhances overall multimodal understanding capabilities.

Our main contributions are summarized as follows: (i) We introduce MM1.5, a family of MLLMs that include both dense models (ranging from 1B to 30B) and MoE variants. (ii) We conduct a thorough empirical study detailing the process and decisions leading to our final design choices. (iii) MM1.5 excels in handling a wide range of multimodal tasks, from general-domain to text-rich image understanding, coarse- to fine-grained understanding, and single- to multi-image reasoning.

2 Recipe for Building MM1.5

In this work, beyond pre-training and SFT stages as in MM1 (McKinzie et al., 2024), we introduce a continual pre-training stage with high-quality OCR data and synthetic captions. As outlined in Figure 1, to obtain the best data recipe,

- We first present comprehensive ablations of our SFT data mixture (Section 2.2). We categorize the SFT data into multiple groups based on the capabilities they aim to support. We carefully evaluate the impact of datasets from each category and adjust the ratio to balance different core capabilities.
- To further enhance model performance, especially for text-rich image understanding, we further ablate the data choices for continual pre-training (Section 2.3). This includes 45M rich OCR data and 7M high-quality captions from public or generated by a MM1-based image captioner.
- We also provide detailed ablation regarding dynamic image splitting, also known as AnyRes (Liu et al., 2024a) (Section 2.4), for high-resolution image comprehension.

Finally, to enhance performance on knowledge-heavy benchmarks like MMMU (Yue et al., 2023a), we further study the impact of pre-training data (Appendix A.2).

2.1 Empirical Setup for Ablations

Unless otherwise noted, we follow the default settings below in our ablation studies.

Model architecture and data preprocessing. We follow MM1 (McKinzie et al., 2024) and use the same architecture, focusing on the 3B dense model for all the ablation studies in this section. Specifically,

- Static image splitting (Lin et al., 2023b) is enabled with 4 sub-image splits (plus an overview image), and each sub-image is resized to 672×672 resolution via position embedding interpolation. Note that we did not use dynamic image splitting during ablation for faster iteration of experiments.
- As to the encoding of multi-image data, we enable image splitting only when the current training sample contains fewer than three images to avoid excessively long sequence lengths.
- Similar to capabilities introduced in Ferret (You et al., 2023), MM1.5 directly supports referring and grounding. When requested, MM1.5 can produce bounding boxes in its textual output to ground its responses. Additionally, the model can interpret references to points and regions in the input image in the form of referring coordinates and bounding boxes.
- The CLIP image encoder and the LLM backbone are based on in-house models, with C-Abstractor (Cha et al., 2024) serving as the vision-language connector.

Model optimization. For both continual pre-training and SFT, we set the batch size as 256. We use the AdaFactor optimizer with a peak learning rate of 1e-5 and a cosine decay of 0. For continual pre-training, we train a maximum of 30k steps. During SFT, all models are optimized for one epoch.

Continual pre-training. Models are initialized with the MM1 pre-trained checkpoint. By default, we conduct continual pre-training on 45M high-resolution OCR data (including PDFA, IDL, Rendered-text (Laurençon et al., 2024a) and DocStruct-4M (Hu et al., 2024a)) at this stage. In each training batch, data is equally sampled from those four datasets. Similar to the SFT stage, we use static image splitting, dividing each image into five sub-images, with each sub-image resized to 672×672 resolution. We find that this high-resolution setup is essential for continual pre-training.

SFT data categorization. Grouping datasets into categories can be helpful for data balancing and simplifying the analysis (Laurençon et al., 2024a; Tong et al., 2024a). At a high level, we cluster datasets into *single-image*, *multi-image*, and *text-only* categories based on the number of images presented in each example. For the single-image group, we further classify each dataset into the following sub-categories: *general*, *text-rich*, *refer&ground*, *science*, *math* and *code*. See Table 5 in Appendix A.3 for the details of each category used for the ablation study, and Figure 8 for an overview of the group categories.

Evaluation benchmarks. We group our benchmarks into categories based on what capabilities a benchmark primarily measures. Our benchmark groups include general, text-rich, refer&ground, knowledge, and multi-image. See Table 6 in Appendix A.4 for more details. We propose *Category Average Score*, the average score of all benchmark numbers for each sub-category, to represent the average performance on that capability. We focus on the categories of general, text-rich, and knowledge, as these capabilities are widely considered essential for MLLMs. To evaluate a model's impact on these capabilities, we refer to a *MMBase* score, defined as the average scores on general, text-rich, and knowledge categories. Details of the evaluation metrics are provided in Appendix A.4.

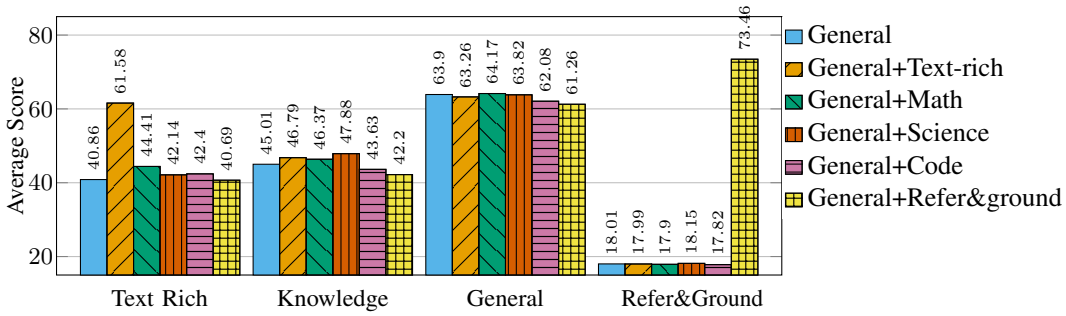

Figure 2: Impact of different SFT data categories to different model capabilities (general, text-rich, knowledge, and refer&ground). Text-rich data significantly improves text-rich and knowledge benchmarks on average. Science data improves knowledge average score. Referring and grounding data enables this capability.

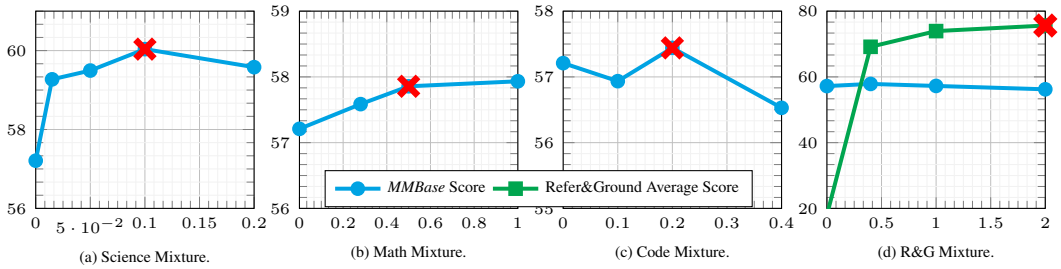

(a) Science Mixture. (b) Math Mixture. (c) Code Mixture. (d) R&G Mixture.

Figure 3: Impact of α (x-axis) for different data categories to a model's different capabilities. The selected ratio is marked with red "x". α denotes the data ratio of the target category (science, math, code, refer&ground (R&G)) when compared with the general category.

2.2 SFT Ablations

To determine the optimal SFT recipe, we first study the impact of different data categories in Section 2.2.1, followed by investigating how to best mix all the data in Section 2.2.2.

2.2.1 Impact of Different Data Categories

In this subsection, we focus on evaluating the single-image data category. We begin by assessing the general data category and then progressively evaluate the impact of adding other sub-categories individually. During training, we mix data from different sub-categories and construct each training batch by randomly sampling data from the corresponding mixture. We compare models using each capability with the *Category Average Score*.

Our results are summarized in Figure 2. We observe that adding text-rich data can significantly improve the performance on text-rich and knowledge benchmarks. The inclusion of math data follows a similar trend, though we observe a lesser degree of improvement in the text-rich average score. When science data is added, we observe the expected improvement in the knowledge benchmarks, alongside a minor improvement in text-rich performance. Adding the code category yields a slight increase in the text-rich average score, while the performance on other benchmarks does not improve. Including the refer&ground data instills the model with referring and grounding capability, but we also observe slight regression in all other capability categories.

2.2.2 Data Mixture Ratio Study

We first study the mixing ratio within the single-image categories. Since directly mixing the general and text-rich data based on their data sizes shows strong results across a variety of benchmarks (see Figure 2), we use this combination as the starting point to study how to mix other categories to this set. Then, we combine the entire single-image set with multi-image and text-only sets with sampling weights of w_{single}, w_{multi} and w_{text}, respectively, where $w_{\text{single}} + w_{\text{multi}} + w_{\text{text}} = 1$.

Mixture of single-image data. Directly mixing all datasets from different categories may not be ideal due to imbalanced numbers of data samples across different sub-categories. For example, the

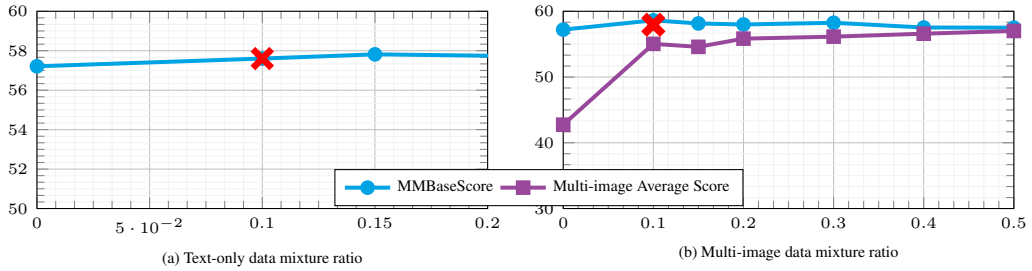

Figure 4: Impact of the mixing ratio for text-only and multi-image SFT data. The selected ratio is marked with red "x".

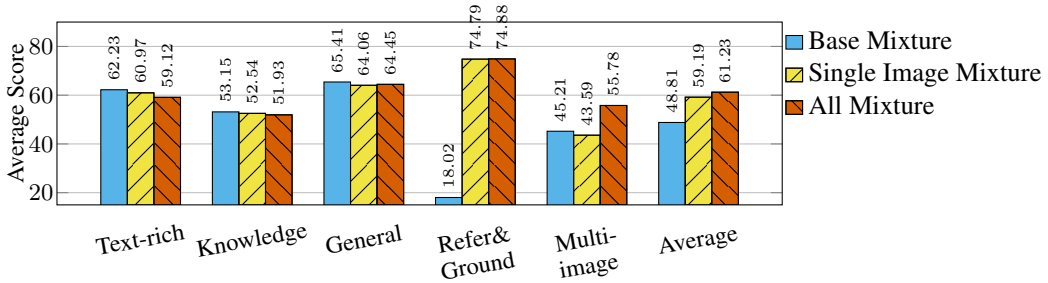

Figure 5: Ablation study of mixing all the SFT data. *Base Mixture* denotes general, text-rich and knowledge (science, math and code). The "Average" column represents the performance averaged across the preceding five benchmark categories.

size of the general data category is around 68× the size of the science data category. In this study, we use the general data category as the reference, and upsample/downsample data from a target category, such that in each training batch, the data ratio from the general and target category is 1:α.

To measure the average impact of α, we propose *MMBase* score, an average over general, text-rich, and knowledge average scores, for model comparison. As shown in Figure 3, we vary the α for different data categories. For science, math, and code categories, we find the best ratio of α to be 0.1, 0.5, and 0.2, respectively. As shown in Section 2.2.1, the refer&ground data is the main driver for improving referring and grounding benchmarks. Therefore, besides the *MMBase* score, we also include the Refer&Ground average score as another metric for the α selection. As summarized in Figure 3(d), the *MMBase* score will drop slightly, while the Refer&Ground average score increases significantly. With that, we select $\alpha = 2.0$ as a good trade-off.

Mixture of single-image, multi-image, and text-only data. Now, we study the mixture ratios, w_{single}, w_{multi} and w_{text}. Enumerating all combinations between the three ratios will incur significant computational cost. Therefore, we instead separately ablate w_{text} and w_{multi} for text-only and multi-image data, respectively, to evaluate how sensitive our model is to these ratios. Finally, w_{single} is determined by $1 - w_{\text{text}} - w_{\text{multi}}$.

Similar to the single-image mixture study, we also start with the combination of general and text-rich data and enumerate different values for w_{multi} and w_{text}. For text-only data, we tested w_{text} from 0 to 0.2. Figure 4(left) shows that varying different values for w_{text} has minor effects on the model's base capabilities in general. We select $w_{\text{text}} = 0.1$ to allocate a higher weight for single-image data for potential performance improvements.

For multi-image data, we use the multi-image average score (evaluated on multi-image benchmarks in Table 6) as an additional metric to assess a model's capability of handling multi-image tasks. Results are summarized in Figure 4(right). We observe that increasing the sampling ratio of multi-image data would introduce a performance drop of the base capabilities as indicated by the decreased number of the *MMBase* score, while the multi-image average score increases. We select $w_{\text{multi}} = 0.1$ since it introduces a surge in the multi-image average score.

Mixing multiple categories. Based on the studies above, we present three mixtures, the *Base* mixture, *Single-image* mixture, and *All* mixture, and analyze their trade-offs. The *Base* mixture includes the

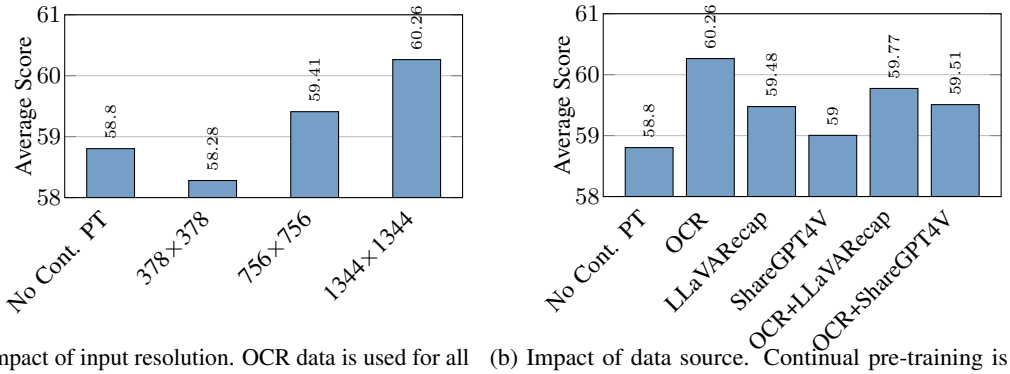

(a) Impact of input resolution. OCR data is used for all the continual pre-training experiments.

(b) Impact of data source. Continual pre-training is conducted in the high-resolution (1344×1344) setting.

Figure 6: Ablation study of continual pre-training. Average Score indicates the *MMBase* score. Cont. PT denotes continual pre-training.

general, text-rich, science ($\alpha_{\text{science}} = 0.1$), math ($\alpha_{\text{math}} = 0.5$) and code ($\alpha_{\text{code}} = 0.2$) data groups. The *Single-image* mixture additionally adds refer&ground data ($\alpha_{\text{rg}} = 2.0$) to the *Base* mixture. *All* mixture includes all data from single-image, multi-image, and text-only data, with $w_{\text{single}} = 0.8$, $w_{\text{multi}} = 0.1$, and $w_{\text{text}} = 0.1$.

Our results are summarized in Figure 5. The first three columns indicate that including refer&ground and multi-image data slightly reduces average performance on text-rich, knowledge, and general benchmarks. The fourth column shows that adding refer&ground data significantly boosts referring and grounding performance, while the fifth column highlights that adding multi-image data greatly improves multi-image benchmarks. The final column reveals that our optimized mixture achieves the best overall performance, balancing all capabilities across benchmarks.

2.3 Continual Pre-training Ablations

Unless otherwise specified, we use OCR data (45M in total), including PDFA, IDL, Rendered-text (Laurençon et al., 2024a) and DocStruct-4M (Hu et al., 2024a) in a high-resolution setting (1344×1344) for continual pre-training. During the SFT stage, all continual pre-trained models in this section are fine-tuned with data from the *Base Mixture* including general, text-rich, knowledge (science, math, and code) with their selected mixture ratios as described in Section 2.2.2.

Impact of image resolution. Intuitively, higher-resolution images are preferable when training with OCR data. We first ablate the impact of image resolution during this stage by setting up two baselines, continual pre-training with 378×378 and 756×756 resolutions, respectively. For the former, we disabled both image splitting and position embedding interpolation (our CLIP image encoder natively supports image resolution of 378×378). For the latter, we enabled image splitting and turn-off position embedding interpolation. The results are shown in Figure 6(a). Note that the final SFT stage always uses image resolution 1344×1344 across these experiments, so the training only differs with respect to the image resolution used in continual pre-training.

We can clearly see that using a setting of 1344×1344 image resolution for continual pre-training achieves the best overall performance. Decreasing resolution consistently leads to lower final scores. In particular, continual pre-training with 378×378 resolution can underperform a model without continual pre-training. We hypothesize this is due to insufficient visible detail at lower resolutions, which may hinder the model's ability to effectively learn from the document-based OCR data in the continual pre-training mixture.

Impact of OCR data and synthetic captions. Besides OCR data, high-quality synthetic image captions (Chen et al., 2023c; Li et al., 2024a) are also widely considered useful for pre-training. To study its impact, we use our default setting except for the data used in continual pre-training. We study two synthetic caption datasets: LLaVA-Recap-3M (Li et al., 2024a) and ShareGPT4V-PT (Chen et al., 2023c), and their combination with our OCR data. When we combine ShareGPT4V-PT or LLaVA-Recap-3M with our OCR data, we equally sample data from individual datasets in each training batch. Results are presented in Figure 6(b). We observe that all continual pre-trained models

Table 1: Ablation on the image resolution and the number of image tokens used in dynamic image splitting. n denotes the total number of sub-images. Row 3: $(n_{\min}, n_{\max}) = (4, 4)$; Row 4-7: $(n_{\min}, n_{\max}) = (9, 9)$. Image encoder resolution: (i) 378×378: no position embedding interpolation; (ii) 672×672: with position embedding interpolation.

Row #	Mode	n	#image tokens (per sub-img / total)	Image Enc. Resolution	Effective Resolution	Text-rich	Knowledge	General	Refer & Ground	Average
1	Static	1	144/144	672×672	0.45MP	49.4	53.6	62.6	71.3	59.2
2		5	144/720	672×672	1.8MP	57.7	53.8	64.4	74.8	62.7
3	Dynamic	5	144/720	672×672	1.8MP	58.6	53.7	64.1	74.0	62.5
4		10	81/810	378×378	1.3MP	57.6	53.3	62.9	74.0	62.0
5		10	81/810	672×672	4.1MP	58.3	53.8	64.3	74.9	62.8
6		10	144/1440	378×378	1.3MP	58.5	54.0	63.2	74.5	62.6
7		10	144/1440	672×672	4.1MP	59.8	54.0	64.5	75.2	63.3

perform better than the baseline without continual pre-training. However, we did not find conclusive evidence that these high-quality synthetic captions improved performance over the arguably simpler OCR data. While prior studies (Li et al., 2024c) show synthetic captions boost performance, our results indicate further investigation into their exact impact is needed.

Therefore, we further investigate the impact of synthetic captions generated through self-training for even larger scales (up to 7M) and more controllable styles, using a pre-trained MM1 model fine-tuned on human-annotated captions, similar to (Fang et al., 2024). This new dataset showed some promise in certain settings, see Appendix A.5 for details. We defer further study of this topic to future work.

2.4 Dynamic Image Splitting Ablations

Dynamic image splitting. Processing high-resolution images is essential for text-rich image understanding. In *static* image splitting (Lin et al., 2023b), images are split into a rigid 2×2 grid, which is often inefficient. Low-resolution images are splitted without any need, and images with non-square aspect ratios can result in sub-images being padding only. Therefore, we adopt a dynamic image splitting approach, which is common in the literature (Li et al., 2024a; Dong et al., 2024b; Hu et al., 2024a; Lin et al., 2023b; Xu et al., 2024c; Zhang et al., 2024d), for MM1.5.

Given a minimum and maximum number of sub-images, $n_{\min}$ and $n_{\max}$, consider the set of all candidate grids $G = \{(n_h, n_w) \in \mathbb{N} \,|\, n_{\min} \leq n_h \cdot n_w \leq n_{\max}\}$. Further, consider the resolution of the vision encoder r, and an input image resolution (h, w). If there is a grid that can cover the image, we choose the grid that minimizes the amount of padding after longer side resizing to the grid, *i.e.*, $g^* = \arg\min_{(n_h,n_w)=g\in G} n_h n_w r^2 - h_g w_g$, subject to $n_h r \geq h_g \geq h$ and $n_w r \geq w_g \geq w$, where h_g, w_g denote the image height and width after longer side resizing the candidate grid. If no such grid exists, we choose the one that minimizes the resolution loss due to scaling the image down and fully covers the longer side resized image. Assume we allow up to 4 sub-images. With a static image splitting approach, all images use the grid $(2, 2)$. The dynamic splitting approach instead allows for the following grids: $\{(1, 1), (1, 2), (2, 1), (1, 3), (3, 1), (1, 4), (4, 1), (2, 2)\}$.

Global-Local Format. In addition to the sub-images, we always feed the original image with a longer side resized to the encoder resolution r to the model. This ensures that the model has a global understanding of the image. If the grid is $(1, 1)$, we omit the overview image. We consider two variants: (i) **before**: the overview image is put before the sub-images; (ii) **after**: the overview image is put after the sub-images. These variants yield different results because an autoregressive mask is used in the LLM decoder, and as such, the choice determines whether the decoder can attend to the overview image when processing the sub-images (i) or attend to the sub-images when processing the overview image (ii).

Sub-image position indicator. Given that an input image is dynamically split into multiple sub-images, we explore whether it is helpful to indicate the position of each sub-image in the original high-resolution image to ensure the model can understand the original 2D image structure. Specifically, we consider two methods.

- **Index.** A tuple of (k, i, j) is used to represent sub-image position information, where k is the zero-indexed image number in the example (assuming there can be multiple images in a training sample), i and j are the one-index row and column id, *e.g.*, $(0, 0, 0)$ is the overview image of image 0, and $(0, 2, 1)$ is the sub-image in the second row and first column, for image 0.

Table 2: Ablation on the image grid configuration $(n_{\min}, n_{\max})$ used in dynamic image splitting.

Row #	$(n_{\min}, n_{\max})$ Train	Inference	DocVQA	InfoVQA	Text-rich	Knowledge	General	Refer & Ground	Average
3B Model Comparison									
1	$(4, 4)$	$(4, 4)$	73.2	48.3	58.6	53.3	64.1	74.0	62.5
2	$(4, 9)$	$(4, 9)$	75.7	53.8	60.0	54.0	63.9	74.6	63.1
3	$(4, 16)$	$(4, 16)$	76.3	55.2	60.7	53.4	64.0	73.8	63.0
4	$(1, 9)$	$(1, 9)$	76.2	54.1	60.4	53.7	62.5	71.5	62.0
5	$(4, 4)$	$(4, 9)$	73.4	52.9	59.7	53.5	63.8	74.0	62.8
6	$(4, 4)$	$(4, 16)$	72.3	53.5	59.6	53.8	63.5	74.0	62.7
7	$(4, 4)$	$(1, 9)$	73.5	52.7	59.8	50.7	62.6	24.5	49.4
7B Model Comparison									
8	$(4, 4)$	$(4, 4)$	77.0	54.3	64.5	61.1	66.8	77.7	67.5
9	$(4, 9)$	$(4, 9)$	81.7	62.1	67.4	60.1	66.6	78.0	68.0
10	$(4, 16)$	$(4, 16)$	83.3	64.1	68.0	58.7	67.7	77.2	67.9

Table 3: Ablation on the sub-image position indicator and the position of the overview image. We set $(n_{\min}, n_{\max}) = (4, 4)$ for experiments.

Row #	Sub-img pos. indicator	Overview image pos.	DocVQA	InfoVQA	Text-rich	Knowledge	General	Refer & Ground	Average
1	none	before	73.2	48.3	58.6	53.5	64.1	74.0	62.5
2	seps	before	74.3	49.7	58.8	53.0	63.8	74.5	62.5
3	index	before	73.4	48.6	58.6	52.7	63.4	74.8	62.4
4	none	after	73.3	49.7	59.2	54.3	64.1	73.8	62.8

- **Seps.** Instead of using indexes, we use three text tokens. Specifically, ':' is the overview image indicator, ',' is the column separator, and '<n>' is the row separator. The latter two tokens are inserted between the set of image tokens corresponding to each sub-image so that the original 2D image structure can be recovered from the flattened image token sequence.

Inference for higher resolution. The tuple $(n_{\min}, n_{\max})$ is used to decide the dynamic image splitting configuration for model training. During inference, it is possible to support even higher-resolution image processing simply by increasing these parameters. For example, we explore training at $(n_{\min}, n_{\max}) = (4, 9)$ to save model training compute, while during inference, we use $(n'_{\min}, n'_{\max}) = (4, 16)$ to process images at even higher effective resolutions.

Findings. We use the final *Single-image Mixture* as our default experiment setting, including general, text-rich, knowledge (science, math and code), and refer&ground data. For fast iteration of experiments, all the models are initialized with the MM1 pre-trained checkpoint without continual pre-training. Following Figure 2, we report the average performance on text-rich, knowledge, general, and refer&ground benchmarks. Our findings are summarized as follows.

- Dynamic image splitting outperforms static splitting in text-rich tasks. Both image resolution and the number of sub-images, along with image token counts, are important (Table 1).
- Regarding image grid configuration (Table 2), dynamic image splitting with a larger $n_{\max}$ significantly improves performance on tasks with unusual aspect ratios, such as DocVQA and InfoVQA, especially when trained natively for it. Grounding performance is highly sensitive to grid size changes, and larger LLM backbones yield greater performance gains, with the 7B model showing larger improvements than the 3B model.
- In terms of position indicators (Table 3), they are not strictly necessary for text-rich tasks, though they can be beneficial for specific tasks like DocVQA and InfoVQA. Additionally, placing the overview image after the sub-images improves performance, as it allows the decoder attention mask to attend to all sub-images more effectively.
- In practice, dynamic image splitting does not significantly increase the number of sub-images to process. In a sample of 100k examples, static splitting generates 500k sub-images, while dynamic splitting with $(n_{\min}, n_{\max}) = (4, 9)$ produces barely more, only 539k images in total.

3 FINAL MODEL AND TRAINING RECIPE

We collect the results from the previous ablations to determine the final recipe for MM1.5 training:

- **Architecture.** We use the same model architecture as MM1 (McKinzie et al., 2024).
- **Data and training pipeline.** As summarized in Figure 1, MM1.5 is trained in three stages:
  - **Pre-training.** The pre-training data comprises three parts: (i) 2B image-text pairs, (ii) 600M interleaved image-text documents with 1B images in total, and (iii) text-only data with 2T tokens. Except for the updated text-only data, the data remains unchanged from MM1 (McKinzie et al., 2024). However, the data ratio has been adjusted from 45:45:10 to 50:10:40, significantly downweighting the interleaved data (from 45% to 10%) while increasing the proportion of text-only data (from 10% to 40%) as discussed in Section A.2.
  - **Continual Pre-training.** We use 45M OCR data to enhance text-rich image understanding. Notably, we do not include additional synthetic image captions based on empirical results.
  - **SFT.** We use the data illustrated in Figure 8 and adopt the mixing ratios studied in Section 2.2.2. Our final mixture consists of 80% single-image data, 10% multi-image data, and 10% text-only SFT data. The single-image data can be further categorized into 37.2% text-rich data, 22.5% refer&ground data (VQA data enriched with bounding boxes and/or point coordinates), 11.3% general data, 5.6% math data, 2.3% code data, and 1.1% science data, totaling 80% of all data.
- **Dynamic high-resolution.** We set the image grid configuration $(n_{\min}, n_{\max}) = (4, 9)$, using an index for the sub-image position indicator and placing the overview image after the sub-images. Dynamic image splitting is only enabled when the current training sample has fewer than three images. The supported resolution reaches up to 4 Megapixels (approximately 2016×2016 for a square image, or 6048×672 for a long image).

We use the same image encoder and the LLM backbone from MM1 (McKinzie et al., 2024), and keep them *unfrozen* during all the model training stages. For pre-training, we follow the exact same learning rate schedule as in MM1 (McKinzie et al., 2024) and 200k training steps with sequence length 4096. For continual pre-training, we use a peak learning rate of 1e-5 with the cosine decay and 30k training steps for all the models (from 1B to 30B). For SFT, we use a peak learning rate of 2e-5 and 23k training steps for all the models.[2]

Mixture-of-Experts (MoE). We introduce two MoE models, a 1B-MoE and a 3B-MoE, with 64 experts replacing dense layers every two layers. We use the same hyperparameters as those applied to the dense models for both scales and top-2 gating with a 0.01 load balance loss to encourage a better expert load balance and a 0.001 router z-loss for training stability (Lepikhin et al., 2021).

3.1 RESULTS

We evaluate our MM1.5 models across 35 multimodal benchmarks using an internal fork of lm-eval-harness (Gao et al., 2023), covering task categories ranging from general multimodal understanding, knowledge, text-rich, referring and grounding, multi-image reasoning, to in-context learning. Detailed results for each capability at various model sizes are further summarized in Table 7, 8, 9, 10, and 11, respectively. Below, we highlight a few key observations from Table 4.

MM1.5 represents a major upgrade over MM1. It delivers improvements across all model sizes and nearly all benchmarks, often by a substantial margin. For instance, MM1.5-30B boosts the MathVista from 39.4 to 55.6, DocVQA from 75.8 to 91.4, and InfoVQA from 47.3 to 67.3. It also offers much enhanced multi-image reasoning capability and introduces new capabilities not present in MM1, such as visual referring & grounding.

Both Dense and MoE model scaling are effective. First, scaling the dense model from 1B to 30B consistently improves performance, with benchmarks like AI2D increasing from 59.3 to 77.2 (see Table 7). Second, both the 1B and 3B MoE models outperform their dense counterparts. Notably, the MM1.5-3B-MoE model can even surpass the MM1.5-7B model in knowledge, general, visual referring and grounding, and multi-image benchmarks, though it falls slightly behind on text-rich benchmarks. This suggests that MoE models show strong potential in integrating diverse capabilities compared to dense models.

[2]All models are trained using the AXLearn framework `https://github.com/apple/axlearn`

Table 4: Comparison with SOTA models on the selected benchmarks. Comparison of more benchmarks and broader baselines can be found in Table 7,8,9, 10 and 11in the Appendix.

Model	Text-rich			Knowledge		General		Refer&Ground		Multi-image	In-context
	TextVQA (val)	DocVQA (test)	InfoVQA (test)	MMMU (val)	MathV (testmini)	SEED^{I}	RealWorldQA	RefCOCO avg	LVIS avg	NLVR2 (val)	VL-ICL avg
1B Model Comparison											
LLaVAOneVision-0.5B	–	70.0	41.8	31.4	34.8	65.5	55.6	–	–	63.4	–
SPHINX-Tiny	57.8	53.0	26.3	–	26.4	–	–	77.2	–	–	–
MM1-1B	68.2	68.4	38.5	33.2	31.1	65.6	51.2	–	51.5	50.9	34.3
MM1.5-1B	72.5	81.0	50.5	35.8	37.2	70.2	53.3	81.4	62.2	79.0	51.0
MM1.5-1B-MoE	76.1	84.8	55.9	41.2	42.9	71.4	57.8	83.9	64.1	83.2	56.0
3B Model Comparison											
IntenVL2-2B	73.4	86.9	58.9	36.3	46.0	70.9	57.4	77.7	51.1	67.4	18.5
MiniCPM-V 2.0-3B	74.1	71.9	37.6	38.2	38.7	67.1	55.8	–	48.0	–	–
Phi-3-Vision-4B	70.1	83.3	49.0	40.4	44.5	71.8	59.4	38.1	54.2	53.6	19.5
MM1-3B	71.9	75.2	44.7	33.9	32.0	68.8	55.8	–	53.4	51.7	37.0
MM1.5-3B	76.5	87.7	58.5	37.1	44.4	72.4	56.9	85.6	67.9	83.8	56.3
MM1.5-3B-MoE	76.8	85.0	53.6	42.9	46.9	73.3	60.7	86.2	66.9	86.0	59.6
7B Model Comparison											
MM1-7B	72.8	76.8	45.5	37.0	35.9	69.9	55.7	–	53.2	59.9	52.8
MM1.5-7B	76.5	88.1	59.5	41.8	47.6	73.4	62.5	86.6	66.4	86.9	56.0
30B Model Comparison											
MM1-30B	73.5	75.8	47.3	44.7	39.4	72.1	59.4	–	53.1	63.1	52.1
MM1.5-30B	79.2	91.4	67.3	47.4	55.6	75.0	69.0	90.1	73.2	90.6	77.6

MM1.5-1B is the state-of-the-art model at the 1B scale. While few models are available at this scale, MM1.5-1B clearly outperforms comparable models such as SPHINX-Tiny (Gao et al., 2024). For reference, MM1.5-1B also significantly surpasses LLaVAOneVision-0.5B (Li et al., 2024c) (*e.g.*, ScienceQA: 67.2 vs. 82.1, DocVQA: 70.0 vs. 81.0, see Table 7 and 8), but it should be stressed that this is of course an even smaller model and as such cannot be directly compared.

MM1.5-3B outperforms MiniCPM-V 2.0 and is competitive with InternVL2 and Phi-3-Vision. Compared to MiniCPM-V 2.0, MM1.5-3B achieves superior results on MathVista (38.7 vs. 44.4) and DocVQA (71.9 vs. 87.7) while also supporting visual referring and grounding, which MiniCPM-V lacks. It surpasses InternVL2-2B on general VQA and, although Phi-3-Vision (4.2B) has an edge on knowledge-based tasks like AI2D as in Table 7, MM1.5-3B excels on text-rich benchmarks (e.g., DocVQA: 83.3 vs. 87.7) and outperforms Phi-3-Vision in referring and grounding (see Table 9), as well as in-context learning tasks (see Table 10).

MM1.5 excels in visual referring and grounding. While most SOTA models focus on improving performance across general, knowledge, and text-rich benchmarks, few have integrated fine-grained image grounding and referring ability into their design. Even GPT-4o relies on set-of-mark prompting to demonstrate visual grounding capabilities. As shown in Table 9, MM1.5-3B outperforms Ferret-7B and is on par with Ferret-13B, both of which are fine-tuned specifically for referring and grounding tasks. Notably, our model inherently possesses these capabilities while still excelling in other areas.

MM1.5 excels in multi-image reasoning and in-context learning. As shown in Table 11, the MM1.5-1B model outperforms LLaVAOneVision-0.5B at the 1B scale. Similarly, at the 3B scale, MM1.5-3B significantly surpasses Phi-3-Vision. Additionally, we evaluate MM1.5's zero-shot transfer capability for video understanding using MVBench (Li et al., 2024h), a benchmark designed for video tasks. Moreover, we evaluate MM1.5's ability of multimodal in-context learning on VL-ICL benchmark (Zong et al., 2024). As shown in Table 10, our models outperform others in in-context learning. In Section A.7, we will further introduce MM1.5-Video, a model variant specifically designed for video understanding.

4 Conclusion and Limitation

In this work, we build on the insights of MM1 (McKinzie et al., 2024) and introduce MM1.5, a family of highly performant generalist MLLMs. While MM1 focused on key pre-training choices, we improve post-pre-training techniques like continual pre-training, dynamic high-resolution image processing, and curation of our supervised fine-tuning datasets. Our extensive ablations show MM1.5 's strong performance in text-rich image understanding, visual grounding, and multi-image reasoning. Like most MLLMs, MM1.5 may produce harmful and counterfactual responses. Future efforts will aim to unify these capabilities for a stronger generalist model, with the hope of benefiting the community beyond specific architectures.

REFERENCES

wendlerc/renderedtext.

Marah Abdin, Sam Ade Jacobs, Ammar Ahmad Awan, Jyoti Aneja, Ahmed Awadallah, Hany Awadalla, Nguyen Bach, Amit Bahree, Arash Bakhtiari, Jianmin Bao, Harkirat Behl, Alon Benhaim, Misha Bilenko, Johan Bjorck, Sébastien Bubeck, Qin Cai, Martin Cai, Caio César Teodoro Mendes, Weizhu Chen, Vishrav Chaudhary, Dong Chen, Dongdong Chen, Yen-Chun Chen, Yi-Ling Chen, Parul Chopra, Xiyang Dai, Allie Del Giorno, Gustavo de Rosa, Matthew Dixon, Ronen Eldan, Victor Fragoso, Dan Iter, Mei Gao, Min Gao, Jianfeng Gao, Amit Garg, Abhishek Goswami, Suriya Gunasekar, Emman Haider, Junheng Hao, Russell J. Hewett, Jamie Huynh, Mojan Javaheripi, Xin Jin, Piero Kauffmann, Nikos Karampatziakis, Dongwoo Kim, Mahoud Khademi, Lev Kurilenko, James R. Lee, Yin Tat Lee, Yuanzhi Li, Yunsheng Li, Chen Liang, Lars Liden, Ce Liu, Mengchen Liu, Weishung Liu, Eric Lin, Zeqi Lin, Chong Luo, Piyush Madan, Matt Mazzola, Arindam Mitra, Hardik Modi, Anh Nguyen, Brandon Norick, Barun Patra, Daniel Perez-Becker, Thomas Portet, Reid Pryzant, Heyang Qin, Marko Radmilac, Corby Rosset, Sambudha Roy, Olatunji Ruwase, Olli Saarikivi, Amin Saied, Adil Salim, Michael Santacroce, Shital Shah, Ning Shang, Hiteshi Sharma, Swadheen Shukla, Xia Song, Masahiro Tanaka, Andrea Tupini, Xin Wang, Lijuan Wang, Chunyu Wang, Yu Wang, Rachel Ward, Guanhua Wang, Philipp Witte, Haiping Wu, Michael Wyatt, Bin Xiao, Can Xu, Jiahang Xu, Weijian Xu, Sonali Yadav, Fan Yang, Jianwei Yang, Ziyi Yang, Yifan Yang, Donghan Yu, Lu Yuan, Chengruidong Zhang, Cyril Zhang, Jianwen Zhang, Li Lyna Zhang, Yi Zhang, Yue Zhang, Yunan Zhang, and Xiren Zhou. Phi-3 technical report: A highly capable language model locally on your phone, 2024a.

Marah Abdin, Sam Ade Jacobs, Ammar Ahmad Awan, Jyoti Aneja, Ahmed Awadallah, Hany Awadalla, Nguyen Bach, Amit Bahree, Arash Bakhtiari, Harkirat Behl, et al. Phi-3 technical report: A highly capable language model locally on your phone. *arXiv preprint arXiv:2404.14219*, 2024b.

Jean-Baptiste Alayrac, Jeff Donahue, Pauline Luc, Antoine Miech, Iain Barr, Yana Hasson, Karel Lenc, Arthur Mensch, Katherine Millican, Malcolm Reynolds, et al. Flamingo: a visual language model for few-shot learning. *NeurIPS*, 2022.

Anthropic. Claude 3 model card, 2023. URL `https://www-cdn.anthropic.com/de8ba9b01c9ab7cbabf5c33b80b7bbc618857627/Model_Card_Claude_3.pdf`. Accessed: 2024-08-13.

Anas Awadalla, Irena Gao, Josh Gardner, Jack Hessel, Yusuf Hanafy, Wanrong Zhu, Kalyani Marathe, Yonatan Bitton, Samir Gadre, Shiori Sagawa, et al. Openflamingo: An open-source framework for training large autoregressive vision-language models. *arXiv preprint arXiv:2308.01390*, 2023.

Anas Awadalla, Le Xue, Oscar Lo, Manli Shu, Hannah Lee, Etash Kumar Guha, Matt Jordan, Sheng Shen, Mohamed Awadalla, Silvio Savarese, et al. Mint-1t: Scaling open-source multimodal data by 10x: A multimodal dataset with one trillion tokens. *arXiv preprint arXiv:2406.11271*, 2024.

Gilles Baechler, Srinivas Sunkara, Maria Wang, Fedir Zubach, Hassan Mansoor, Vincent Etter, Victor Carbune, Jason Lin, Jindong Chen, and Abhanshu Sharma. Screenai: A vision-language model for ui and infographics understanding. In *IJCAI*, 2024.

Jinze Bai, Shuai Bai, Shusheng Yang, Shijie Wang, Sinan Tan, Peng Wang, Junyang Lin, Chang Zhou, and Jingren Zhou. Qwen-vl: A frontier large vision-language model with versatile abilities. *arXiv preprint arXiv:2308.12966*, 2023.

Jonas Belouadi, Anne Lauscher, and Steffen Eger. Automatikz: Text-guided synthesis of scientific vector graphics with tikz. *arXiv preprint arXiv:2310.00367*, 2023.

Lucas Beyer, Andreas Steiner, André Susano Pinto, Alexander Kolesnikov, Xiao Wang, Daniel Salz, Maxim Neumann, Ibrahim Alabdulmohsin, Michael Tschannen, Emanuele Bugliarello, et al. Paligemma: A versatile 3b vlm for transfer. *arXiv preprint arXiv:2407.07726*, 2024.

Ali Furkan Biten, Ruben Tito, Andres Mafla, Lluis Gomez, Marçal Rusinol, Ernest Valveny, CV Jawahar, and Dimosthenis Karatzas. Scene text visual question answering. In *ICCV*, 2019.

Mu Cai, Jianwei Yang, Jianfeng Gao, and Yong Jae Lee. Matryoshka multimodal models. *arXiv preprint arXiv:2405.17430*, 2024.

Junbum Cha, Wooyoung Kang, Jonghwan Mun, and Byungseok Roh. Honeybee: Locality-enhanced projector for multimodal llm. In *CVPR*, 2024.

Jun Chen, Deyao Zhu, Xiaoqian Shen, Xiang Li, Zechun Liu, Pengchuan Zhang, Raghuraman Krishnamoorthi, Vikas Chandra, Yunyang Xiong, and Mohamed Elhoseiny. Minigpt-v2: large language model as a unified interface for vision-language multi-task learning. *arXiv preprint arXiv:2310.09478*, 2023a.

Keqin Chen, Zhao Zhang, Weili Zeng, Richong Zhang, Feng Zhu, and Rui Zhao. Shikra: Unleashing multimodal llm's referential dialogue magic. *arXiv preprint arXiv:2306.15195*, 2023b.

Kezhen Chen, Rahul Thapa, Rahul Chalamala, Ben Athiwaratkun, Shuaiwen Leon Song, and James Zou. Dragonfly: Multi-resolution zoom supercharges large visual-language model. *arXiv preprint arXiv:2406.00977*, 2024a.

Lin Chen, Jisong Li, Xiaoyi Dong, Pan Zhang, Conghui He, Jiaqi Wang, Feng Zhao, and Dahua Lin. Sharegpt4v: Improving large multi-modal models with better captions. *arXiv preprint arXiv:2311.12793*, 2023c.

Wenhu Chen, Hongmin Wang, Jianshu Chen, Yunkai Zhang, Hong Wang, Shiyang Li, Xiyou Zhou, and William Yang Wang. Tabfact: A large-scale dataset for table-based fact verification. *arXiv preprint arXiv:1909.02164*, 2019.

Xinlei Chen, Hao Fang, Tsung-Yi Lin, Ramakrishna Vedantam, Saurabh Gupta, Piotr Dollár, and C Lawrence Zitnick. Microsoft coco captions: Data collection and evaluation server. *arXiv preprint arXiv:1504.00325*, 2015.

Zhe Chen, Weiyun Wang, Hao Tian, Shenglong Ye, Zhangwei Gao, Erfei Cui, Wenwen Tong, Kongzhi Hu, Jiapeng Luo, Zheng Ma, et al. How far are we to gpt-4v? closing the gap to commercial multimodal models with open-source suites. *arXiv preprint arXiv:2404.16821*, 2024b.

Zhe Chen, Jiannan Wu, Wenhai Wang, Weijie Su, Guo Chen, Sen Xing, Muyan Zhong, Qinglong Zhang, Xizhou Zhu, Lewei Lu, et al. Internvl: Scaling up vision foundation models and aligning for generic visual-linguistic tasks. In *CVPR*, 2024c.

Zhiyu Chen, Wenhu Chen, Charese Smiley, Sameena Shah, Iana Borova, Dylan Langdon, Reema Moussa, Matt Beane, Ting-Hao Huang, Bryan Routledge, et al. Finqa: A dataset of numerical reasoning over financial data. *arXiv preprint arXiv:2109.00122*, 2021.

Zesen Cheng, Sicong Leng, Hang Zhang, Yifei Xin, Xin Li, Guanzheng Chen, Yongxin Zhu, Wenqi Zhang, Ziyang Luo, Deli Zhao, and Lidong Bing. VideoLLaMA 2: Advancing spatial-temporal modeling and audio understanding in video-llms. *arXiv preprint arXiv:2406.07476*, 2024.

Zhoujun Cheng, Haoyu Dong, Zhiruo Wang, Ran Jia, Jiaqi Guo, Yan Gao, Shi Han, Jian-Guang Lou, and Dongmei Zhang. Hitab: A hierarchical table dataset for question answering and natural language generation. *arXiv preprint arXiv:2108.06712*, 2021.

Xiaoyi Dong, Pan Zhang, Yuhang Zang, Yuhang Cao, Bin Wang, Linke Ouyang, Songyang Zhang, Haodong Duan, Wenwei Zhang, Yining Li, et al. Internlm-xcomposer2-4khd: A pioneering large vision-language model handling resolutions from 336 pixels to 4k hd. *arXiv preprint arXiv:2404.06512*, 2024a.

Xiaoyi Dong, Pan Zhang, Yuhang Zang, Yuhang Cao, Bin Wang, Linke Ouyang, Songyang Zhang, Haodong Duan, Wenwei Zhang, Yining Li, et al. Internlm-xcomposer2-4khd: A pioneering large vision-language model handling resolutions from 336 pixels to 4k hd. *arXiv preprint arXiv:2404.06512*, 2024b.

Haodong Duan, Junming Yang, Yuxuan Qiao, Xinyu Fang, Lin Chen, Yuan Liu, Xiaoyi Dong, Yuhang Zang, Pan Zhang, Jiaqi Wang, Dahua Lin, and Kai Chen. Vlmevalkit: An open-source toolkit for evaluating large multi-modality models, 2024. URL `https://arxiv.org/abs/2407.11691`.

Abhimanyu Dubey, Abhinav Jauhri, Abhinav Pandey, Abhishek Kadian, Ahmad Al-Dahle, Aiesha Letman, Akhil Mathur, Alan Schelten, Amy Yang, Angela Fan, et al. The llama 3 herd of models. *arXiv preprint arXiv:2407.21783*, 2024.

Yunhao Fang, Ligeng Zhu, Yao Lu, Yan Wang, Pavlo Molchanov, Jang Hyun Cho, Marco Pavone, Song Han, and Hongxu Yin. $vila^2$: Vila augmented vila. *arXiv preprint arXiv:2407.17453*, 2024.

Maxwell Forbes, Christine Kaeser-Chen, Piyush Sharma, and Serge Belongie. Neural naturalist: Generating fine-grained image comparisons. *arXiv preprint arXiv:1909.04101*, 2019.

Chaoyou Fu, Peixian Chen, Yunhang Shen, Yulei Qin, Mengdan Zhang, Xu Lin, Jinrui Yang, Xiawu Zheng, Ke Li, Xing Sun, Yunsheng Wu, and Rongrong Ji. Mme: A comprehensive evaluation benchmark for multimodal large language models. *arXiv preprint arXiv:2306.13394*, 2024a.

Chaoyou Fu, Yuhan Dai, Yondong Luo, Lei Li, Shuhuai Ren, Renrui Zhang, Zihan Wang, Chenyu Zhou, Yunhang Shen, Mengdan Zhang, et al. Video-MME: The first-ever comprehensive evaluation benchmark of multi-modal llms in video analysis. *arXiv preprint arXiv:2405.21075*, 2024b.

Stephanie Fu*, Netanel Tamir*, Shobhita Sundaram*, Lucy Chai, Richard Zhang, Tali Dekel, and Phillip Isola. Dreamsim: Learning new dimensions of human visual similarity using synthetic data. *arXiv preprint arXiv:2306.09344*, 2023.

Xingyu Fu, Yushi Hu, Bangzheng Li, Yu Feng, Haoyu Wang, Xudong Lin, Dan Roth, Noah A Smith, Wei-Chiu Ma, and Ranjay Krishna. Blink: Multimodal large language models can see but not perceive. *arXiv preprint arXiv:2404.12390*, 2024c.

Leo Gao, Jonathan Tow, Baber Abbasi, Stella Biderman, Sid Black, Anthony DiPofi, Charles Foster, Laurence Golding, Jeffrey Hsu, Alain Le Noac'h, Haonan Li, Kyle McDonell, Niklas Muennighoff, Chris Ociepa, Jason Phang, Laria Reynolds, Hailey Schoelkopf, Aviya Skowron, Lintang Sutawika, Eric Tang, Anish Thite, Ben Wang, Kevin Wang, and Andy Zou. A framework for few-shot language model evaluation, 12 2023. URL https://zenodo.org/records/10256836.

Peng Gao, Renrui Zhang, Chris Liu, Longtian Qiu, Siyuan Huang, Weifeng Lin, Shitian Zhao, Shijie Geng, Ziyi Lin, Peng Jin, et al. Sphinx-x: Scaling data and parameters for a family of multi-modal large language models. *arXiv preprint arXiv:2402.05935*, 2024.

Chunjiang Ge, Sijie Cheng, Ziming Wang, Jiale Yuan, Yuan Gao, Jun Song, Shiji Song, Gao Huang, and Bo Zheng. Convllava: Hierarchical backbones as visual encoder for large multimodal models. *arXiv preprint arXiv:2405.15738*, 2024.

Tom Gunter, Zirui Wang, Chong Wang, Ruoming Pang, Andy Narayanan, Aonan Zhang, Bowen Zhang, Chen Chen, Chung-Cheng Chiu, David Qiu, et al. Apple intelligence foundation language models. *arXiv preprint arXiv:2407.21075*, 2024.

Agrim Gupta, Piotr Dollár, and Ross B. Girshick. LVIS: A dataset for large vocabulary instance segmentation. In *CVPR*, 2019.

Muyang He, Yexin Liu, Boya Wu, Jianhao Yuan, Yueze Wang, Tiejun Huang, and Bo Zhao. Efficient multimodal learning from data-centric perspective. *arXiv preprint arXiv:2402.11530*, 2024.

Musashi Hinck, Matthew L Olson, David Cobbley, Shao-Yen Tseng, and Vasudev Lal. Llava-gemma: Accelerating multimodal foundation models with a compact language model. *arXiv preprint arXiv:2404.01331*, 2024.

Wenyi Hong, Weihan Wang, Ming Ding, Wenmeng Yu, Qingsong Lv, Yan Wang, Yean Cheng, Shiyu Huang, Junhui Ji, Zhao Xue, et al. Cogvlm2: Visual language models for image and video understanding. *arXiv preprint arXiv:2408.16500*, 2024a.

Wenyi Hong, Weihan Wang, Qingsong Lv, Jiazheng Xu, Wenmeng Yu, Junhui Ji, Yan Wang, Zihan Wang, Yuxiao Dong, Ming Ding, et al. Cogagent: A visual language model for gui agents. In *CVPR*, 2024b.

Yu-Chung Hsiao, Fedir Zubach, Maria Wang, and Jindong Chen. Screenqa: Large-scale question-answer pairs over mobile app screenshots. *arXiv preprint arXiv:2209.08199*, 2022.

Anwen Hu, Haiyang Xu, Jiabo Ye, Ming Yan, Liang Zhang, Bo Zhang, Chen Li, Ji Zhang, Qin Jin, Fei Huang, et al. mplug-docowl 1.5: Unified structure learning for ocr-free document understanding. *arXiv preprint arXiv:2403.12895*, 2024a.

Anwen Hu, Haiyang Xu, Jiabo Ye, Ming Yan, Liang Zhang, Bo Zhang, Chen Li, Ji Zhang, Qin Jin, Fei Huang, et al. mplug-docowl 1.5: Unified structure learning for ocr-free document understanding. *arXiv preprint arXiv:2403.12895*, 2024b.

Mingxin Huang, Yuliang Liu, Dingkang Liang, Lianwen Jin, and Xiang Bai. Mini-monkey: Alleviate the sawtooth effect by multi-scale adaptive cropping. *arXiv preprint arXiv:2408.02034*, 2024.

Shaohan Huang, Li Dong, Wenhui Wang, Yaru Hao, Saksham Singhal, Shuming Ma, Tengchao Lv, Lei Cui, Owais Khan Mohammed, Barun Patra, et al. Language is not all you need: Aligning perception with language models. *NeurIPS*, 2023.

Drew A Hudson and Christopher D Manning. Gqa: A new dataset for real-world visual reasoning and compositional question answering. *CVPR*, 2019.

Raisa Islam and Owana Marzia Moushi. Gpt-4o: The cutting-edge advancement in multimodal llm. *Authorea Preprints*, 2024.

Harsh Jhamtani and Taylor Berg-Kirkpatrick. Learning to describe differences between pairs of similar images. *arXiv preprint arXiv:1808.10584*, 2018.

Dongfu Jiang, Xuan He, Huaye Zeng, Cong Wei, Max Ku, Qian Liu, and Wenhu Chen. Mantis: Interleaved multi-image instruction tuning. *arXiv preprint arXiv:2405.01483*, 2024.

Peng Jin, Ryuichi Takanobu, Wancai Zhang, Xiaochun Cao, and Li Yuan. Chat-univi: Unified visual representation empowers large language models with image and video understanding. In *CVPR*, 2024a.

Yizhang Jin, Jian Li, Yexin Liu, Tianjun Gu, Kai Wu, Zhengkai Jiang, Muyang He, Bo Zhao, Xin Tan, Zhenye Gan, et al. Efficient multimodal large language models: A survey. *arXiv preprint arXiv:2405.10739*, 2024b.

Justin Johnson, Bharath Hariharan, Laurens Van Der Maaten, Li Fei-Fei, C Lawrence Zitnick, and Ross Girshick. Clevr: A diagnostic dataset for compositional language and elementary visual reasoning. In *CVPR*, 2017.

Kushal Kafle, Brian Price, Scott Cohen, and Christopher Kanan. Dvqa: Understanding data visualizations via question answering. In *CVPR*, 2018.

Mehran Kazemi, Hamidreza Alvari, Ankit Anand, Jialin Wu, Xi Chen, and Radu Soricut. Geomverse: A systematic evaluation of large models for geometric reasoning. *arXiv preprint arXiv:2312.12241*, 2023.

Sahar Kazemzadeh, Vicente Ordonez, Mark Matten, and Tamara Berg. Referitgame: Referring to objects in photographs of natural scenes. In *EMNLP*, 2014.

Aniruddha Kembhavi, Mike Salvato, Eric Kolve, Minjoon Seo, Hannaneh Hajishirzi, and Ali Farhadi. A diagram is worth a dozen images. In *ECCV*, 2016a.

Aniruddha Kembhavi, Mike Salvato, Eric Kolve, Minjoon Seo, Hannaneh Hajishirzi, and Ali Farhadi. A diagram is worth a dozen images. In *ECCV*, 2016b.

Geewook Kim, Teakgyu Hong, Moonbin Yim, JeongYeon Nam, Jinyoung Park, Jinyeong Yim, Wonseok Hwang, Sangdoo Yun, Dongyoon Han, and Seunghyun Park. Ocr-free document understanding transformer. In *ECCV*, 2022.

Wonkyun Kim, Changin Choi, Wonseok Lee, and Wonjong Rhee. An image grid can be worth a video: Zero-shot video question answering using a vlm. *arXiv preprint arXiv:2403.18406*, 2024.

Ranjay Krishna, Yuke Zhu, Oliver Groth, Justin Johnson, Kenji Hata, Joshua Kravitz, Stephanie Chen, Yannis Kalantidis, Li-Jia Li, David A Shamma, et al. Visual genome: Connecting language and vision using crowdsourced dense image annotations. *IJCV*, 2017.

Xin Lai, Zhuotao Tian, Yukang Chen, Yanwei Li, Yuhui Yuan, Shu Liu, and Jiaya Jia. Lisa: Reasoning segmentation via large language model. In *CVPR*, 2024.

Hugo Laurençon, Andrés Marafioti, Victor Sanh, and Léo Tronchon. Building and better understanding vision-language models: insights and future directions. *arXiv preprint arXiv:2408.12637*, 2024a.

Hugo Laurençon, Lucile Saulnier, Léo Tronchon, Stas Bekman, Amanpreet Singh, Anton Lozhkov, Thomas Wang, Siddharth Karamcheti, Alexander Rush, Douwe Kiela, et al. Obelics: An open web-scale filtered dataset of interleaved image-text documents. *NeurIPS*, 2024b.

Hugo Laurençon, Léo Tronchon, Matthieu Cord, and Victor Sanh. What matters when building vision-language models? *arXiv preprint arXiv:2405.02246*, 2024a.

Hugo Laurençon, Léo Tronchon, and Victor Sanh. Unlocking the conversion of web screenshots into html code with the websight dataset. *arXiv preprint arXiv:2403.09029*, 2024b.

Dmitry Lepikhin, HyoukJoong Lee, Yuanzhong Xu, Dehao Chen, Orhan Firat, Yanping Huang, Maxim Krikun, Noam Shazeer, and Zhifeng Chen. {GS}hard: Scaling giant models with conditional computation and automatic sharding. In *ICLR*, 2021.

Bo Li, Yuanhan Zhang, Liangyu Chen, Jinghao Wang, Fanyi Pu, Jingkang Yang, Chunyuan Li, and Ziwei Liu. Mimic-it: Multi-modal in-context instruction tuning. *arXiv preprint arXiv:2306.05425*, 2023a.

Bo Li, Hao Zhang, Kaichen Zhang, Dong Guo, Yuanhan Zhang, Renrui Zhang, Feng Li, Ziwei Liu, and Chunyuan Li. Llava-next: What else influences visual instruction tuning beyond data?, May 2024a. URL https://llava-vl.github.io/blog/2024-05-25-llava-next-ablations/.

Bo Li, Peiyuan Zhang, Kaichen Zhang, Fanyi Pu, Xinrun Du, Yuhao Dong, Haotian Liu, Yuanhan Zhang, Ge Zhang, Chunyuan Li, and Ziwei Liu. Lmms-eval: Accelerating the development of large multimodal models, March 2024b. URL https://github.com/EvolvingLMMs-Lab/lmms-eval.

Bo Li, Yuanhan Zhang, Dong Guo, Renrui Zhang, Feng Li, Hao Zhang, Kaichen Zhang, Yanwei Li, Ziwei Liu, and Chunyuan Li. Llava-onevision: Easy visual task transfer. *arXiv preprint arXiv:2408.03326*, 2024c.

Bohao Li, Rui Wang, Guangzhi Wang, Yuying Ge, Yixiao Ge, and Ying Shan. Seed-bench: Benchmarking multimodal llms with generative comprehension. *arXiv preprint arXiv:2307.16125*, 2023b.

Chunyuan Li, Zhe Gan, Zhengyuan Yang, Jianwei Yang, Linjie Li, Lijuan Wang, Jianfeng Gao, et al. Multimodal foundation models: From specialists to general-purpose assistants. *Foundations and Trends® in Computer Graphics and Vision*, 16(1-2):1–214, 2024d.

Feng Li, Renrui Zhang, Hao Zhang, Yuanhan Zhang, Bo Li, Wei Li, Zejun Ma, and Chunyuan Li. Llava-next-interleave: Tackling multi-image, video, and 3d in large multimodal models. *arXiv preprint arXiv:2407.07895*, 2024e.

Feng Li, Renrui Zhang, Hao Zhang, Yuanhan Zhang, Bo Li, Wei Li, Zejun Ma, and Chunyuan Li. Llava-next: Tackling multi-image, video, and 3d in large multimodal models, June 2024f. URL https://llava-vl.github.io/blog/2024-06-16-llava-next-interleave/.

Gang Li and Yang Li. Spotlight: Mobile UI understanding using vision-language models with a focus. In *ICLR*, 2023.

Jiachen Li, Xinyao Wang, Sijie Zhu, Chia-Wen Kuo, Lu Xu, Fan Chen, Jitesh Jain, Humphrey Shi, and Longyin Wen. Cumo: Scaling multimodal llm with co-upcycled mixture-of-experts. *arXiv preprint arXiv:2405.05949*, 2024g.

Jiapeng Li, Ping Wei, Wenjuan Han, and Lifeng Fan. IntentQA: Context-aware video intent reasoning. In *ICCV*, 2023c.

Junnan Li, Dongxu Li, Silvio Savarese, and Steven Hoi. Blip-2: Bootstrapping language-image pre-training with frozen image encoders and large language models. In *ICML*, 2023d.

KunChang Li, Yinan He, Yi Wang, Yizhuo Li, Wenhai Wang, Ping Luo, Yali Wang, Limin Wang, and Yu Qiao. Videochat: Chat-centric video understanding. *arXiv preprint arXiv:2305.06355*, 2023e.

Kunchang Li, Yali Wang, Yinan He, Yizhuo Li, Yi Wang, Yi Liu, Zun Wang, Jilan Xu, Guo Chen, Ping Luo, Limin Wang, and Yu Qiao. Mvbench: A comprehensive multi-modal video understanding benchmark. *arXiv preprint arXiv:2311.17005*, 2023f.

Kunchang Li, Yali Wang, Yinan He, Yizhuo Li, Yi Wang, Yi Liu, Zun Wang, Jilan Xu, Guo Chen, Ping Luo, et al. Mvbench: A comprehensive multi-modal video understanding benchmark. In *CVPR*, 2024h.

Lei Li, Yuqi Wang, Runxin Xu, Peiyi Wang, Xiachong Feng, Lingpeng Kong, and Qi Liu. Multimodal arxiv: A dataset for improving scientific comprehension of large vision-language models. *arXiv preprint arXiv:2403.00231*, 2024i.

Qingyun Li, Zhe Chen, Weiyun Wang, Wenhai Wang, Shenglong Ye, Zhenjiang Jin, Guanzhou Chen, Yinan He, Zhangwei Gao, Erfei Cui, et al. Omnicorpus: An unified multimodal corpus of 10 billion-level images interleaved with text. *arXiv preprint arXiv:2406.08418*, 2024j.

Wentong Li, Yuqian Yuan, Jian Liu, Dongqi Tang, Song Wang, Jianke Zhu, and Lei Zhang. Token-packer: Efficient visual projector for multimodal llm. *arXiv preprint arXiv:2407.02392*, 2024k.

Yang Li, Gang Li, Luheng He, Jingjie Zheng, Hong Li, and Zhiwei Guan. Widget captioning: Generating natural language description for mobile user interface elements. In Bonnie Webber, Trevor Cohn, Yulan He, and Yang Liu (eds.), *EMNLP*, 2020.

Yanwei Li, Chengyao Wang, and Jiaya Jia. LLaMA-VID: An image is worth 2 tokens in large language models. *arXiv preprint arXiv:2311.17043*, 2023g.

Yanwei Li, Yuechen Zhang, Chengyao Wang, Zhisheng Zhong, Yixin Chen, Ruihang Chu, Shaoteng Liu, and Jiaya Jia. Mini-gemini: Mining the potential of multi-modality vision language models. *arXiv preprint arXiv:2403.18814*, 2024l.

Yifan Li, Yifan Du, Kun Zhou, Jinpeng Wang, Wayne Xin Zhao, and Ji-Rong Wen. Evaluating object hallucination in large vision-language models. *arXiv preprint arXiv:2305.10355*, 2023h.

Zhang Li, Biao Yang, Qiang Liu, Zhiyin Ma, Shuo Zhang, Jingxu Yang, Yabo Sun, Yuliang Liu, and Xiang Bai. Monkey: Image resolution and text label are important things for large multi-modal models. *arXiv preprint arXiv:2311.06607*, 2023i.

Wing Lian, Bleys Goodson, Eugene Pentland, Austin Cook, Chanvichet Vong, and "Teknium". Openorca: An open dataset of gpt augmented flan reasoning traces. `https://https://huggingface.co/Open-Orca/OpenOrca`, 2023.

Bin Lin, Bin Zhu, Yang Ye, Munan Ning, Peng Jin, and Li Yuan. Video-llava: Learning united visual representation by alignment before projection. *arXiv preprint arXiv:2311.10122*, 2023a.

Bin Lin, Zhenyu Tang, Yang Ye, Jiaxi Cui, Bin Zhu, Peng Jin, Junwu Zhang, Munan Ning, and Li Yuan. Moe-llava: Mixture of experts for large vision-language models. *arXiv preprint arXiv:2401.15947*, 2024a.

Ji Lin, Hongxu Yin, Wei Ping, Pavlo Molchanov, Mohammad Shoeybi, and Song Han. Vila: On pre-training for visual language models. In *CVPR*, 2024b.

Tsung-Yi Lin, Michael Maire, Serge Belongie, James Hays, Pietro Perona, Deva Ramanan, Piotr Dollár, and C Lawrence Zitnick. Microsoft coco: Common objects in context. In *ECCV*, 2014.

Ziyi Lin, Chris Liu, Renrui Zhang, Peng Gao, Longtian Qiu, Han Xiao, Han Qiu, Chen Lin, Wenqi Shao, Keqin Chen, et al. Sphinx: The joint mixing of weights, tasks, and visual embeddings for multi-modal large language models. *arXiv preprint arXiv:2311.07575*, 2023b.

Haotian Liu, Chunyuan Li, Yuheng Li, and Yong Jae Lee. Llava-1.5: Improved baselines with visual instruction tuning. *arXiv preprint arXiv:2310.03744*, 2023a.

Haotian Liu, Chunyuan Li, Qingyang Wu, and Yong Jae Lee. Visual instruction tuning. *arXiv preprint arXiv:2304.08485*, 2023b.

Haotian Liu, Chunyuan Li, Yuheng Li, Bo Li, Yuanhan Zhang, Sheng Shen, and Yong Jae Lee. Llava-next: Improved reasoning, ocr, and world knowledge, 2024a.

Yuliang Liu, Zhang Li, Mingxin Huang, Biao Yang, Wenwen Yu, Chunyuan Li, Xucheng Yin, Cheng lin Liu, Lianwen Jin, and Xiang Bai. On the hidden mystery of ocr in large multimodal models. *arXiv preprint arXiv:2305.07895*, 2024b.

Haoyu Lu, Wen Liu, Bo Zhang, Bingxuan Wang, Kai Dong, Bo Liu, Jingxiang Sun, Tongzheng Ren, Zhuoshu Li, Hao Yang, Yaofeng Sun, Chengqi Deng, Hanwei Xu, Zhenda Xie, and Chong Ruan. Deepseek-vl: Towards real-world vision-language understanding. *arXiv preprint arXiv:2403.05525*, 2024.

Pan Lu, Ran Gong, Shibiao Jiang, Liang Qiu, Siyuan Huang, Xiaodan Liang, and Song-Chun Zhu. Inter-gps: Interpretable geometry problem solving with formal language and symbolic reasoning. In *ACL*, 2021a.

Pan Lu, Liang Qiu, Jiaqi Chen, Tony Xia, Yizhou Zhao, Wei Zhang, Zhou Yu, Xiaodan Liang, and Song-Chun Zhu. Iconqa: A new benchmark for abstract diagram understanding and visual language reasoning. In *NeurIPS Track on Datasets and Benchmarks*, 2021b.

Pan Lu, Swaroop Mishra, Tony Xia, Liang Qiu, Kai-Wei Chang, Song-Chun Zhu, Oyvind Tafjord, Peter Clark, and Ashwin Kalyan. Learn to explain: Multimodal reasoning via thought chains for science question answering. In *NeurIPS*, 2022.

Pan Lu, Hritik Bansal, Tony Xia, Jiacheng Liu, Chunyuan Li, Hannaneh Hajishirzi, Hao Cheng, Kai-Wei Chang, Michel Galley, and Jianfeng Gao. Mathvista: Evaluating mathematical reasoning of foundation models in visual contexts. *arXiv preprint arXiv:2310.02255*, 2023a.

Pan Lu, Liang Qiu, Kai-Wei Chang, Ying Nian Wu, Song-Chun Zhu, Tanmay Rajpurohit, Peter Clark, and Ashwin Kalyan. Dynamic prompt learning via policy gradient for semi-structured mathematical reasoning. In *ICLR*, 2023b.

Ziyang Luo, Can Xu, Pu Zhao, Qingfeng Sun, Xiubo Geng, Wenxiang Hu, Chongyang Tao, Jing Ma, Qingwei Lin, and Daxin Jiang. Wizardcoder: Empowering code large language models with evol-instruct. *arXiv preprint arXiv:2306.08568*, 2023.

Fan Ma, Xiaojie Jin, Heng Wang, Yuchen Xian, Jiashi Feng, and Yi Yang. Vista-llama: Reducing hallucination in video language models via equal distance to visual tokens. In *CVPR*, 2024.

Muhammad Maaz, Hanoona Rasheed, Salman Khan, and Fahad Shahbaz Khan. Video-ChatGPT: Towards detailed video understanding via large vision and language models. In *ACL*, 2024.

Karttikeya Mangalam, Raiymbek Akshulakov, and Jitendra Malik. Egoschema: A diagnostic benchmark for very long-form video language understanding. *NeurIPS*, 2024.

Kenneth Marino, Mohammad Rastegari, Ali Farhadi, and Roozbeh Mottaghi. Ok-vqa: A visual question answering benchmark requiring external knowledge. In *CVPR*, 2019.

Ahmed Masry, Do Xuan Long, Jia Qing Tan, Shafiq Joty, and Enamul Hoque. Chartqa: A benchmark for question answering about charts with visual and logical reasoning. *arXiv preprint arXiv:2203.10244*, 2022.

Minesh Mathew, Dimosthenis Karatzas, and CV Jawahar. Docvqa: A dataset for vqa on document images. In *WACV*, 2021.

Minesh Mathew, Viraj Bagal, Rubèn Tito, Dimosthenis Karatzas, Ernest Valveny, and CV Jawahar. Infographicvqa. In *WACV*, 2022.

Brandon McKinzie, Zhe Gan, Jean-Philippe Fauconnier, Sam Dodge, Bowen Zhang, Philipp Dufter, Dhruti Shah, Xianzhi Du, Futang Peng, Floris Weers, et al. Mm1: Methods, analysis & insights from multimodal llm pre-training. *arXiv preprint arXiv:2403.09611*, 2024.

Lingchen Meng, Jianwei Yang, Rui Tian, Xiyang Dai, Zuxuan Wu, Jianfeng Gao, and Yu-Gang Jiang. Deepstack: Deeply stacking visual tokens is surprisingly simple and effective for lmms. *arXiv preprint arXiv:2406.04334*, 2024.

C Mike, H Matt, M Ankit, X Jianwei, W Jun, S Sam, G Ali, W Patrick, Z Matei, and X Reynold. Free dolly: Introducing the world's first truly open instruction-tuned llm, 2023.

Anand Mishra, Shashank Shekhar, Ajeet Kumar Singh, and Anirban Chakraborty. Ocr-vqa: Visual question answering by reading text in images. In *ICDAR*, 2019.

Arindam Mitra, Hamed Khanpour, Corby Rosset, and Ahmed Awadallah. Orca-math: Unlocking the potential of slms in grade school math. *arXiv preprint arXiv:2402.14830*, 2024.

Varun K Nagaraja, Vlad I Morariu, and Larry S Davis. Modeling context between objects for referring expression understanding. In *ECCV*, 2016.

Jason Obeid and Enamul Hoque. Chart-to-text: Generating natural language descriptions for charts by adapting the transformer model. *arXiv preprint arXiv:2010.09142*, 2020.

OpenAI. Gpt-4 vision. OpenAI, 2024. https://openai.com/research/gpt-4-vision.

Panupong Pasupat and Percy Liang. Compositional semantic parsing on semi-structured tables. *arXiv preprint arXiv:1508.00305*, 2015.

Zhiliang Peng, Wenhui Wang, Li Dong, Yaru Hao, Shaohan Huang, Shuming Ma, and Furu Wei. Kosmos-2: Grounding multimodal large language models to the world. *arXiv preprint arXiv:2306.14824*, 2023.

Bryan A Plummer, Liwei Wang, Chris M Cervantes, Juan C Caicedo, Julia Hockenmaier, and Svetlana Lazebnik. Flickr30k entities: Collecting region-to-phrase correspondences for richer image-to-sentence models. In *ICCV*, 2015.

Hanoona Rasheed, Muhammad Maaz, Sahal Shaji, Abdelrahman Shaker, Salman Khan, Hisham Cholakkal, Rao M Anwer, Eric Xing, Ming-Hsuan Yang, and Fahad S Khan. Glamm: Pixel grounding large multimodal model. In *CVPR*, 2024.

Machel Reid, Nikolay Savinov, Denis Teplyashin, Dmitry Lepikhin, Timothy Lillicrap, Jean-baptiste Alayrac, Radu Soricut, Angeliki Lazaridou, Orhan Firat, Julian Schrittwieser, et al. Gemini 1.5: Unlocking multimodal understanding across millions of tokens of context. *arXiv preprint arXiv:2403.05530*, 2024.

Zhongwei Ren, Zhicheng Huang, Yunchao Wei, Yao Zhao, Dongmei Fu, Jiashi Feng, and Xiaojie Jin. Pixellm: Pixel reasoning with large multimodal model. In *CVPR*, 2024.

Eldon Schoop, Xin Zhou, Gang Li, Zhourong Chen, Bjoern Hartmann, and Yang Li. Predicting and explaining mobile ui tappability with vision modeling and saliency analysis. In *Proceedings of the 2022 CHI Conference on Human Factors in Computing Systems*. Association for Computing Machinery, 2022.

Dustin Schwenk, Apoorv Khandelwal, Christopher Clark, Kenneth Marino, and Roozbeh Mottaghi. A-okvqa: A benchmark for visual question answering using world knowledge. In *ECCV*, 2022.

Shuai Shao, Zeming Li, Tianyuan Zhang, Chao Peng, Gang Yu, Xiangyu Zhang, Jing Li, and Jian Sun. Objects365: A large-scale, high-quality dataset for object detection. In *ICCV*, 2019.

Min Shi, Fuxiao Liu, Shihao Wang, Shijia Liao, Subhashree Radhakrishnan, De-An Huang, Hongxu Yin, Karan Sapra, Yaser Yacoob, Humphrey Shi, et al. Eagle: Exploring the design space for multimodal llms with mixture of encoders. *arXiv preprint arXiv:2408.15998*, 2024.

Chenglei Si, Yanzhe Zhang, Zhengyuan Yang, Ruibo Liu, and Diyi Yang. Design2code: How far are we from automating front-end engineering? *arXiv preprint arXiv:2403.03163*, 2024.

Oleksii Sidorov, Ronghang Hu, Marcus Rohrbach, and Amanpreet Singh. Textcaps: a dataset for image captioningwith reading comprehension. In *ECCV*, 2020.

Amanpreet Singh, Vivek Natarajan, Meet Shah, Yu Jiang, Xinlei Chen, Dhruv Batra, Devi Parikh, and Marcus Rohrbach. Towards vqa models that can read. In *CVPR*, 2019.

Enxin Song, Wenhao Chai, Tian Ye, Jenq-Neng Hwang, Xi Li, and Gaoang Wang. Moviechat+: Question-aware sparse memory for long video question answering. *arXiv preprint arXiv:2404.17176*, 2024.

Tomasz Stanisławek, Filip Graliński, Anna Wróblewska, Dawid Lipiński, Agnieszka Kaliska, Paulina Rosalska, Bartosz Topolski, and Przemysław Biecek. Kleister: key information extraction datasets involving long documents with complex layouts. In *International Conference on Document Analysis and Recognition*, 2021.

Alane Suhr, Stephanie Zhou, Ally Zhang, Iris Zhang, Huajun Bai, and Yoav Artzi. A corpus for reasoning about natural language grounded in photographs. *arXiv preprint arXiv:1811.00491*, 2018.

Quan Sun, Yufeng Cui, Xiaosong Zhang, Fan Zhang, Qiying Yu, Zhengxiong Luo, Yueze Wang, Yongming Rao, Jingjing Liu, Tiejun Huang, and Xinlong Wang. Generative multimodal models are in-context learners. *arXiv preprint arXiv:2312.13286*, 2023a.

Quan Sun, Qiying Yu, Yufeng Cui, Fan Zhang, Xiaosong Zhang, Yueze Wang, Hongcheng Gao, Jingjing Liu, Tiejun Huang, and Xinlong Wang. Generative pretraining in multimodality. *arXiv preprint arXiv:2307.05222*, 2023b.

Quan Sun, Yufeng Cui, Xiaosong Zhang, Fan Zhang, Qiying Yu, Yueze Wang, Yongming Rao, Jingjing Liu, Tiejun Huang, and Xinlong Wang. Generative multimodal models are in-context learners. In *CVPR*, 2024.

Stacey Svetlichnaya. Deepform: Understand structured documents at scale, 2020.

Ryota Tanaka, Kyosuke Nishida, and Sen Yoshida. Visualmrc: Machine reading comprehension on document images. In *AAAI*, 2021.

Benny J. Tang, Angie Boggust, and Arvind Satyanarayan. VisText: A Benchmark for Semantically Rich Chart Captioning. In *ACL*, 2023.

Jingqun Tang, Chunhui Lin, Zhen Zhao, Shu Wei, Binghong Wu, Qi Liu, Hao Feng, Yang Li, Siqi Wang, Lei Liao, et al. Textsquare: Scaling up text-centric visual instruction tuning. *arXiv preprint arXiv:2404.12803*, 2024.

Gemini Team, Rohan Anil, Sebastian Borgeaud, Yonghui Wu, Jean-Baptiste Alayrac, Jiahui Yu, Radu Soricut, Johan Schalkwyk, Andrew M Dai, Anja Hauth, et al. Gemini: a family of highly capable multimodal models. *arXiv preprint arXiv:2312.11805*, 2023.

Qwen team. Qwen2-vl, August 2024. URL `https://qwenlm.github.io/blog/qwen2-vl/`.

Shengbang Tong, Ellis Brown, Penghao Wu, Sanghyun Woo, Manoj Middepogu, Sai Charitha Akula, Jihan Yang, Shusheng Yang, Adithya Iyer, Xichen Pan, Austin Wang, Rob Fergus, Yann LeCun, and Saining Xie. Cambrian-1: A fully open, vision-centric exploration of multimodal llms. *arXiv preprint arXiv:2406.16860*, 2024a.

Shengbang Tong, Zhuang Liu, Yuexiang Zhai, Yi Ma, Yann LeCun, and Saining Xie. Eyes wide shut? exploring the visual shortcomings of multimodal llms. In *CVPR*, 2024b.

Maria Tsimpoukelli, Jacob L Menick, Serkan Cabi, SM Eslami, Oriol Vinyals, and Felix Hill. Multimodal few-shot learning with frozen language models. *NeurIPS*, 2021.

Bryan Wang, Gang Li, Xin Zhou, Zhourong Chen, Tovi Grossman, and Yang Li. Screen2words: Automatic mobile ui summarization with multimodal learning. In *The 34th Annual ACM Symposium on User Interface Software and Technology*. Association for Computing Machinery, 2021.

Fei Wang, Xingyu Fu, James Y Huang, Zekun Li, Qin Liu, Xiaogeng Liu, Mingyu Derek Ma, Nan Xu, Wenxuan Zhou, Kai Zhang, et al. Muirbench: A comprehensive benchmark for robust multi-image understanding. *arXiv preprint arXiv:2406.09411*, 2024.

Weihan Wang, Qingsong Lv, Wenmeng Yu, Wenyi Hong, Ji Qi, Yan Wang, Junhui Ji, Zhuoyi Yang, Lei Zhao, Xixuan Song, et al. Cogvlm: Visual expert for pretrained language models. *arXiv preprint arXiv:2311.03079*, 2023a.

Wenhai Wang, Zhe Chen, Xiaokang Chen, Jiannan Wu, Xizhou Zhu, Gang Zeng, Ping Luo, Tong Lu, Jie Zhou, Yu Qiao, et al. Visionllm: Large language model is also an open-ended decoder for vision-centric tasks. *arXiv preprint arXiv:2305.11175*, 2023b.

Bo Wu, Shoubin Yu, Zhenfang Chen, Joshua B Tenenbaum, and Chuang Gan. Star: A benchmark for situated reasoning in real-world videos. *arXiv preprint arXiv:2405.09711*, 2024a.

Haoning Wu, Hanwei Zhu, Zicheng Zhang, Erli Zhang, Chaofeng Chen, Liang Liao, Chunyi Li, Annan Wang, Wenxiu Sun, Qiong Yan, et al. Towards open-ended visual quality comparison. *arXiv preprint arXiv:2402.16641*, 2024b.

x.ai. Grok-1.5 vision preview. URL `https://x.ai/blog/grok-1.5v`.

Junbin Xiao, Xindi Shang, Angela Yao, and Tat-Seng Chua. NExT-QA: Next phase of question-answering to explaining temporal actions. In *CVPR*, 2021a.

Junbin Xiao, Xindi Shang, Angela Yao, and Tat-Seng Chua. Next-qa: Next phase of question-answering to explaining temporal actions. In *CVPR*, 2021b.

Lin Xu, Yilin Zhao, Daquan Zhou, Zhijie Lin, See Kiong Ng, and Jiashi Feng. Pllava: Parameter-free llava extension from images to videos for video dense captioning. *arXiv preprint arXiv:2404.16994*, 2024a.

Mingze Xu, Mingfei Gao, Zhe Gan, Hong-You Chen, Zhengfeng Lai, Haiming Gang, Kai Kang, and Afshin Dehghan. SlowFast-LLaVA: A strong training-free baseline for video large language models. *arXiv preprint arXiv:2407.15841*, 2024b.

Ruyi Xu, Yuan Yao, Zonghao Guo, Junbo Cui, Zanlin Ni, Chunjiang Ge, Tat-Seng Chua, Zhiyuan Liu, Maosong Sun, and Gao Huang. Llava-uhd: an lmm perceiving any aspect ratio and high-resolution images. *arXiv preprint arXiv:2403.11703*, 2024c.

Le Xue, Manli Shu, Anas Awadalla, Jun Wang, An Yan, Senthil Purushwalkam, Honglu Zhou, Viraj Prabhu, Yutong Dai, Michael S Ryoo, et al. xgen-mm (blip-3): A family of open large multimodal models. *arXiv preprint arXiv:2408.08872*, 2024.

Jianwei Yang, Hao Zhang, Feng Li, Xueyan Zou, Chunyuan Li, and Jianfeng Gao. Set-of-mark prompting unleashes extraordinary visual grounding in gpt-4v. *arXiv preprint arXiv:2310.11441*, 2023.

Huanjin Yao, Wenhao Wu, Taojiannan Yang, YuXin Song, Mengxi Zhang, Haocheng Feng, Yifan Sun, Zhiheng Li, Wanli Ouyang, and Jingdong Wang. Dense connector for mllms. *arXiv preprint arXiv:2405.13800*, 2024a.

Yuan Yao, Tianyu Yu, Ao Zhang, Chongyi Wang, Junbo Cui, Hongji Zhu, Tianchi Cai, Haoyu Li, Weilin Zhao, Zhihui He, et al. Minicpm-v: A gpt-4v level mllm on your phone. *arXiv preprint arXiv:2408.01800*, 2024b.

Haoxuan You, Haotian Zhang, Zhe Gan, Xianzhi Du, Bowen Zhang, Zirui Wang, Liangliang Cao, Shih-Fu Chang, and Yinfei Yang. Ferret: Refer and ground anything anywhere at any granularity. *arXiv preprint arXiv:2310.07704*, 2023.

Keen You, Haotian Zhang, Eldon Schoop, Floris Weers, Amanda Swearngin, Jeffrey Nichols, Yinfei Yang, and Zhe Gan. Ferret-ui: Grounded mobile ui understanding with multimodal llms. *arXiv preprint arXiv:2404.05719*, 2024.

Peter Young, Alice Lai, Micah Hodosh, and Julia Hockenmaier. From image descriptions to visual denotations: New similarity metrics for semantic inference over event descriptions. *TACL*, 2014.

Licheng Yu, Patrick Poirson, Shan Yang, Alexander C Berg, and Tamara L Berg. Modeling context in referring expressions. In *ECCV*, 2016.

Weihao Yu, Zhengyuan Yang, Linjie Li, Jianfeng Wang, Kevin Lin, Zicheng Liu, Xinchao Wang, and Lijuan Wang. Mm-vet: Evaluating large multimodal models for integrated capabilities. *arXiv preprint arXiv:2308.02490*, 2023.

Zhou Yu, Dejing Xu, Jun Yu, Ting Yu, Zhou Zhao, Yueting Zhuang, and Dacheng Tao. ActivityNet-QA: A dataset for understanding complex web videos via question answering. In *AAAI*, 2019.

Yuqian Yuan, Wentong Li, Jian Liu, Dongqi Tang, Xinjie Luo, Chi Qin, Lei Zhang, and Jianke Zhu. Osprey: Pixel understanding with visual instruction tuning. In *CVPR*, 2024.

Xiang Yue, Yuansheng Ni, Kai Zhang, Tianyu Zheng, Ruoqi Liu, Ge Zhang, Samuel Stevens, Dongfu Jiang, Weiming Ren, Yuxuan Sun, et al. Mmmu: A massive multi-discipline multimodal understanding and reasoning benchmark for expert agi. *arXiv preprint arXiv:2311.16502*, 2023a.

Xiang Yue, Xingwei Qu, Ge Zhang, Yao Fu, Wenhao Huang, Huan Sun, Yu Su, and Wenhu Chen. Mammoth: Building math generalist models through hybrid instruction tuning. *arXiv preprint arXiv:2309.05653*, 2023b.

Yuhang Zang, Wei Li, Jun Han, Kaiyang Zhou, and Chen Change Loy. Contextual object detection with multimodal large language models. *arXiv preprint arXiv:2305.18279*, 2023.

Chi Zhang, Feng Gao, Baoxiong Jia, Yixin Zhu, and Song-Chun Zhu. Raven: A dataset for relational and analogical visual reasoning. In *CVPR*, 2019.

Haotian Zhang, Haoxuan You, Philipp Dufter, Bowen Zhang, Chen Chen, Hong-You Chen, Tsu-Jui Fu, William Yang Wang, Shih-Fu Chang, Zhe Gan, et al. Ferret-v2: An improved baseline for referring and grounding with large language models. *arXiv preprint arXiv:2404.07973*, 2024a.

Pan Zhang, Xiaoyi Dong, Yuhang Zang, Yuhang Cao, Rui Qian, Lin Chen, Qipeng Guo, Haodong Duan, Bin Wang, Linke Ouyang, et al. Internlm-xcomposer-2.5: A versatile large vision language model supporting long-contextual input and output. *arXiv preprint arXiv:2407.03320*, 2024b.

Ruohong Zhang, Liangke Gui, Zhiqing Sun, Yihao Feng, Keyang Xu, Yuanhan Zhang, Di Fu, Chunyuan Li, Alexander Hauptmann, Yonatan Bisk, et al. Direct preference optimization of video large multimodal models from language model reward. *arXiv preprint arXiv:2404.01258*, 2024c.

Shilong Zhang, Peize Sun, Shoufa Chen, Min Xiao, Wenqi Shao, Wenwei Zhang, Kai Chen, and Ping Luo. Gpt4roi: Instruction tuning large language model on region-of-interest. *arXiv preprint arXiv:2307.03601*, 2023.

Yi-Fan Zhang, Qingsong Wen, Chaoyou Fu, Xue Wang, Zhang Zhang, Liang Wang, and Rong Jin. Beyond llava-hd: Diving into high-resolution large multimodal models. *arXiv preprint arXiv:2406.08487*, 2024d.

Zicheng Zhang, Haoning Wu, Erli Zhang, Guangtao Zhai, and Weisi Lin. A benchmark for multi-modal foundation models on low-level vision: from single images to pairs. *arXiv preprint arXiv:2402.07116*, 2024e.

Yang Zhao, Zhijie Lin, Daquan Zhou, Zilong Huang, Jiashi Feng, and Bingyi Kang. Bubogpt: Enabling visual grounding in multi-modal llms. *arXiv preprint arXiv:2307.08581*, 2023.

Tianyu Zheng, Ge Zhang, Tianhao Shen, Xueling Liu, Bill Yuchen Lin, Jie Fu, Wenhu Chen, and Xiang Yue. Opencodeinterpreter: Integrating code generation with execution and refinement. *arXiv preprint arXiv:2402.14658*, 2024.

Victor Zhong, Caiming Xiong, and Richard Socher. Seq2sql: Generating structured queries from natural language using reinforcement learning. *arXiv preprint arXiv:1709.00103*, 2017.

Baichuan Zhou, Ying Hu, Xi Weng, Junlong Jia, Jie Luo, Xien Liu, Ji Wu, and Lei Huang. Tinyllava: A framework of small-scale large multimodal models. *arXiv preprint arXiv:2402.14289*, 2024.

Deyao Zhu, Jun Chen, Xiaoqian Shen, Xiang Li, and Mohamed Elhoseiny. Minigpt-4: Enhancing vision-language understanding with advanced large language models. *arXiv preprint arXiv:2304.10592*, 2023.

Fengbin Zhu, Wenqiang Lei, Youcheng Huang, Chao Wang, Shuo Zhang, Jiancheng Lv, Fuli Feng, and Tat-Seng Chua. TAT-QA: A question answering benchmark on a hybrid of tabular and textual content in finance. In *ACL*, 2021.

Yongshuo Zong, Ondrej Bohdal, and Timothy Hospedales. Vl-icl bench: The devil in the details of benchmarking multimodal in-context learning. *arXiv preprint arXiv:2403.13164*, 2024.

A APPENDIX

A.1 RELATED WORK

Multimodal Large Language Models (MLLMs) (OpenAI, 2024; Islam & Moushi, 2024; Team et al., 2023; Li et al., 2024d; Huang et al., 2023) have recently emerged as a significant area of research focus. The development of MLLMs can be traced back to Frozen (Tsimpoukelli et al., 2021) and Flamingo (Alayrac et al., 2022; Awadalla et al., 2023), with more recent advancements such as LLaVA (Liu et al., 2023b) and MiniGPT-4 (Zhu et al., 2023) introducing the concept of visual instruction tuning. The past year has witnessed a boom of open-source MLLMs, some of which claim to rival GPT-4o on certain benchmarks. Notable examples include Emu2 (Sun et al., 2023b; 2024), VILA (Lin et al., 2024b), Idefics2/3 (Laurençon et al., 2024a; Laurençon et al., 2024a), Cambrian-1 (Tong et al., 2024a), InternLM-XComposer-2.5 (Dong et al., 2024a; Zhang et al., 2024b), InternVL2 (Chen et al., 2024c;b), MiniCPM-V (Yao et al., 2024b), CogVLM2 (Wang et al., 2023a; Hong et al., 2024a), BLIP-3 (Li et al., 2023d; Xue et al., 2024), LLaVA-OneVision (Li et al., 2024e), Llama3.1-V (Dubey et al., 2024), and the latest Qwen2-VL (Bai et al., 2023).

Research in MLLMs has expanded across several fronts: (i) scaling up the pre-training data (Lin et al., 2024b; McKinzie et al., 2024; Xue et al., 2024; Awadalla et al., 2024; Li et al., 2024j) and supervised instruction-tuning data (Hu et al., 2024b; Tang et al., 2024; Laurençon et al., 2024a; Tong et al., 2024a); (ii) enhancing high-resolution image comprehension (Lin et al., 2023b; Li et al., 2023i; Liu et al., 2024a; Dong et al., 2024a; Gao et al., 2024; Ge et al., 2024; Chen et al., 2024a; Zhang et al., 2024d; Xu et al., 2024c; Li et al., 2024l); (iii) exploring various vision encoders (Tong et al., 2024b; Shi et al., 2024) and vision-language connectors (Cha et al., 2024; Yao et al., 2024a; Li et al., 2024k; Cai et al., 2024); (iv) using mixture-of-experts (Lin et al., 2024a; Li et al., 2024g); (v) extending LLaVA-like architectures to region-level (Wang et al., 2023b; Zhao et al., 2023; Zang et al., 2023; Peng et al., 2023; Chen et al., 2023b; Zhang et al., 2023; You et al., 2023; Zhang et al., 2024a) and pixel-level (Lai et al., 2024; Rasheed et al., 2024; Yuan et al., 2024; Ren et al., 2024) understanding, multi-image reasoning (Jiang et al., 2024; Li et al., 2024e), UI comprehension (You et al., 2024; Hong et al., 2024b), and video understanding (Lin et al., 2023a; Xu et al., 2024a;b), among others.

Among the extensive body of literature on MLLMs, MM1.5 distinguishes itself as a significant upgrade over its predecessor, MM1 (McKinzie et al., 2024). The MM1.5 model family integrates a diverse set of core capabilities, including text-rich image understanding, visual referring and grounding, and multi-image reasoning. In contrast, recent general-purpose MLLMs such as Cambrian-1 (Tong et al., 2024a) and LLaVA-OneVision (Li et al., 2024e) have shown less satisfactory performance in handling referring and grounding tasks, and GPT-4o has to rely on set-of-mark (SoM) prompting (Yang et al., 2023) to understand image regions.

While several recent works have open-sourced detailed SFT data mixtures for public use (Laurençon et al., 2024a; Tong et al., 2024a), the precise impact of each data category and the best recipe to combine them remain under-explored. This is particularly true for models requiring diverse capabilities. MM1.5 stands out by providing a comprehensive empirical study that presents mature recipes for building performant MLLMs. The extension of MM1.5 to mobile UI understanding further enhances the uniqueness of this work.

Another emerging trend in the field is the development of lightweight MLLMs for potential edge deployment (Jin et al., 2024b; Huang et al., 2024; Beyer et al., 2024; Lu et al., 2024; Hinck et al., 2024; Li et al., 2024l; Zhou et al., 2024; He et al., 2024). In MM1.5, models with 1B and 3B parameters are offered, which outperform similar-sized models, such as Phi-3-Vision (Abdin et al., 2024b) and MiniCPM-V (Yao et al., 2024b).

A.2 PRE-TRAINING ABLATIONS

Beyond the SFT and continual pre-training, we emphasize the importance of large-scale, task-specific data used during pre-training in establishing robust foundations for models to effectively handle diverse tasks. For knowledge-heavy benchmarks like MMMU (Yue et al., 2023a), we found that model performance is highly sensitive to its text comprehension capabilities. The LLM's ability to understand and process textual content is pivotal in addressing the complex reasoning and knowledge-representation challenges posed by these benchmarks, as also observed in Cambrian-1 (Tong et al., 2024a).

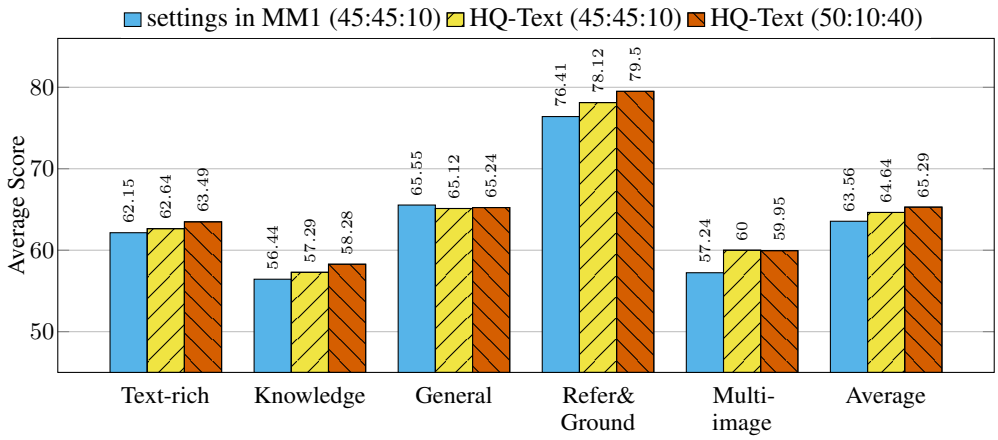

Figure 7: Performance comparison of all categories across different text-only data and pre-training data ratio. The figure highlights the performance improvement when replacing with *HQ-Text* data and the additional gains achieved by adjusting the ratio to 50:10:40. Note that the default setting for continual pre-training (OCR) and *All Mixture* for SFT are used for all models.

We incorporated a higher-quality and more diverse set of text-only datasets, referred to as *HQ-Text*, introduced by (Gunter et al., 2024), during the pre-training phase. These datasets were specifically curated to enhance the model's language capabilities by providing deeper and more varied textual contexts, with a focus on general knowledge, mathematics, and coding. This update aims to strengthen the model's ability in language-based reasoning.

As shown in Figure 7, by simply replacing with the new data, the average score on knowledge improves by 0.85 points.

In conjunction with the text-only datasets and the latest SFT recipes discussed in Section 2.2, we further refined our pre-training data composition. The original data ratio proposed in MM1 (McKinzie et al., 2024) was 45:45:10 for image-caption, interleaved image-text, and text-only data, respectively. Further experiments revealed that decreasing the amount of interleaved pre-training data and, respectively, increasing the weight of text-only data to a ratio of 50:10:40 resulted in improved performance across most tasks after SFT. We note that in contrast to pre-training ablations in MM1, for MM1.5, we conduct evaluations on downstream benchmarks post SFT to select our final pre-training mixture. We hypothesize that relying primarily on few-shot pre-training metrics may not be ideal, as the improvements on such evaluations may not effectively transfer to downstream performance. Our newly optimized data mix for MM1.5 not only enhances multimodal capabilities but also strengthens language understanding, leading to superior overall performance across benchmarks.

With the updated mixture, performance on text-rich average increased by 0.85, knowledge average by 0.99, and refer&ground tasks by around 1.4, as shown in Figure 7. Although there was a slight decrease of 0.05 on multi-image datasets due to the lower weighting of interleaved data, we consider this trade-off reasonable for maintaining strong performance across all tasks.

A.3 Details of SFT Data for Ablation & Final SFT Mixture

As presented in Table 5, we use a subset of our final SFT data when conducting the ablation study. The MM1.5 final mixture is presented in Figure 8.

A.4 MM1.5 Benchmark Details

Benchmarks used for MM1.5 evaluation are summarized in Table 6, where for each *Category Average Score*, we directly calculate the average of each metric number within that capability category as follows, with detailed evaluation metrics listed in Table 6.

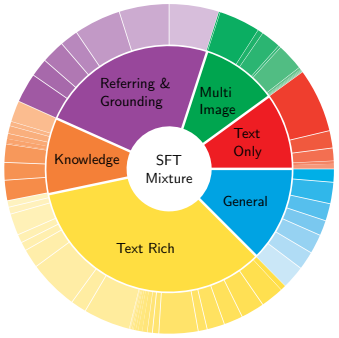

General

- LLaVA v1.5 VQAv2 OKVQA Marino et al. (2019); Liu et al. (2023a) (91.8k)
- LLaVA v1.5 A-OKVQA Schwenk et al. (2022) (66.2k)
- LLaVA Complex Reasoning Liu et al. (2023b) (76.6k)
- LLaVA 1.5 conversation Liu et al. (2023a) (56.7k)
- LLaVA v1.5 GQA Hudson & Manning (2019); Liu et al. (2023a) (72.1k)
- Coco Captions Chen et al. (2015) (82.8k)
- ShareGPT-4V Chen et al. (2023c) (96.1k)

Text Rich

- Synthdog-En Kim et al. (2022) (500k)
- ScreenQA Hsiao et al. (2022) (80.8k)
- WikiTQ Pasupat & Liang (2015) (38.2k)
- TabMWP Lu et al. (2023b) (22.7k)
- ST-VQA Biten et al. (2019) (17.2k)
- VisText Tang et al. (2023) (10k)
- DeepForm Svetlichnaya (2020) (7k)
- HiTab Cheng et al. (2021) (2.5k)
- ChartQA Masry et al. (2022) (66.7k)
- InfoVQA Mathew et al. (2022) (52.3k)
- TabFact Chen et al. (2019) (91.6k)
- KleisterCharity Stanisławek et al. (2021) (27.7k)
- TextVQA Singh et al. (2019) (34.6k)
- TextCaps Sidorov et al. (2020) (22k)
- ArxivQA Li et al. (2024i) (100k)
- WikiSQL Zhong et al. (2017) (75k)
- Chart2Text Obeid & Hoque (2020) (27k)
- TextVQA Singh et al. (2019) (34.6k)
- RenderedText ren (10k)
- FinQA Chen et al. (2021) (5.3k)
- TAT-QA Zhu et al. (2021) (2.2k)
- DVQA Kafle et al. (2018) (200k)
- DocVQA Mathew et al. (2021) (128.5k)
- WikiTable (35.8k) Pasupat & Liang (2015)
- VisualMRC Tanaka et al. (2021) (24.5k)
- OCRVQA Mishra et al. (2019) (80k)

Knowledge (Math/Science/Code)

- RAVEN Zhang et al. (2019) (42k)
- AI2D Kembhavi et al. (2016a) (3.2k)
- DaTikZ Belouadi et al. (2023) (48k)
- CLEVR Johnson et al. (2017) (70k)
- Inter-GPS Lu et al. (2021a) (1.3k)
- ScienceQA Lu et al. (2022) (5k)
- Design2Code Si et al. (2024) (0.5k)
- IconQA Lu et al. (2021b) (27.3k)
- GeomVerse Kazemi et al. (2023) (9.3k)
- WebSight Laurençon et al. (2024b) (10k)

Referring & Grounding

- GRIT-Flickr30k You et al. (2023); Plummer et al. (2015) (200.8k)
- GRIT-Visual Genome You et al. (2023); Krishna et al. (2017) (267.6k)
- GRIT-Refcoco You et al. (2023); Lin et al. (2014); Yu et al. (2016); Nagaraja et al. (2016) (210k)
- GRIT-Region reasoning You et al. (2023) (76.6k)
- GRIT-Spatial Negative Mining You et al. (2023); Shao et al. (2019) (213.6k)

Multi-image

- DreamSim Jiang et al. (2024); Fu* et al. (2023) (15.9k)
- NLVR2 Jiang et al. (2024); Suhr et al. (2018) (86.4k)
- Star Jiang et al. (2024); Wu et al. (2024a) (3k)
- Birds-to-Words Jiang et al. (2024); Forbes et al. (2019) (2.6k)
- IconQA Jiang et al. (2024); Lu et al. (2021b) (64.5k)
- Spot-the-diff Jiang et al. (2024); Jhamtani & Berg-Kirkpatrick (2018) (8k)
- ICL-Instruct† (0.4k)
- Coinstruct Jiang et al. (2024); Wu et al. (2024b) (132.3k)
- MultiVQA Jiang et al. (2024) (5k)
- NExT-QA Jiang et al. (2024); Xiao et al. (2021b) (3.9k)
- Coco instruct interleaved† (2.1k)

Text

- OrcaMath Mitra et al. (2024) (200k)
- Dolly Mike et al. (2023) (11k)
- OpenOrca Lian et al. (2023) (994k)
- WizardCoder Luo et al. (2023) (43k)
- MathInstruct Yue et al. (2023b) (262k)
- OpenCodeInterpreter Zheng et al. (2024) (66k)

Figure 8: A high-quality data mixture used for MM1.5 supervised fine-tuning, including (i) single-image data for enhanced math/science reasoning, text-rich image understanding, and visual referring and grounding, (ii) multi-image data, and (iii) text-only data. (†) denotes in-house datasets with curation details in Appendix A.9.

Table 5: Overview of the SFT data used in ablation study.

Data category	Sub-category	Datasets	# QA
Single-image	**General**	LLaVA Complex Reasoning, LLaVA Conversation, ShareGPT-4v, Coco Caption, LLaVA v1.5 VQAv2 OKVQA, LLaVA v1.5 GQA, LLaVA v1.5 A-OKVQA	542K
	Text Rich	OCRVQA, Synthdog-En, TextCaps, TextVQA, DVQA, ChartQA, DocVQA, InfoVQA, VisualMRC, WikiTQ, DeepForm, KleisterCharity, TabFact	1.3M
	Refer&Ground	GRIT-Visual Genome, GRIT-Region reasoning, GRIT-Flickr30k, GRIT-Refcoco, GRIT-Spatial Negative Mining	1.08M
	Science	AI2D, ScienceQA	8K
	Math	GeomVerse, CLEVER, IconQA, RAVEN, Inter-GPS	150K
	Code	WebSight, DaTikZ, Design2Code	58K
Multi-image	–	DreamSim, NLVR2, Star, Birds-to-Words, IconQA, Spot-the-diff, ICL-instruct, Coinstruct, MultiVQA, NExT-QA, Coco Instruct Interleaved	324K
Text-only	–	Dolly, OpenOrca, MathInstruct, WizardCoder, OrcaMath, OpenCodeInterpreter	1.71M

- **General Average Score**: average score of the corresponding metric scores from MME-Normalize[3], Seed-IMG, POPE, LLaVA^{W}, MM-Vet and RealWorldQA.
- **Text-rich Average Score**: average score of the corresponding metric scores from WTQ, TabFact, OCRBench[4], ChartQA[5], TextVQA, DocVQA and InfoVQA.

[3]MME-Normalize is (MME-Perception + MME-Cognition)/2800 $\times 100\%$.
[4]The accuracy of OCRbench is the total score normalized by 1000 $\times 100\%$.
[5]Average of human part accuracy and augmented part accuracy.

Table 6: Details of benchmarks and their metrics used in MM1.5 ablation study. Benchmarks marked with (†) are excluded from the category average.

Category	Benchmark	Metric
General	MME Fu et al. (2024a)	Normalized Accuracy
	SEED Li et al. (2023b)	Seed-IMG
	POPE Li et al. (2023h)	Average of random, popular and adversarial
	LLaVA-Bench (Wild) Liu et al. (2023b)	GPT-assisted score
	MM-Vet Yu et al. (2023)	GPT-assisted score
	RealWorldQA x.ai	Accuracy
Text-rich	WTQ Pasupat & Liang (2015)	Accuracy
	TabFact Chen et al. (2019)	Accuracy
	OCRBench Liu et al. (2024b)	Accuracy
	ChartQA Masry et al. (2022)	Accuracy
	TextVQA Singh et al. (2019)	VQA Open Flamingo Accuracy
	DocVQA Mathew et al. (2021)	ANLS Score
	InfoVQA Mathew et al. (2022)	ANLS Score
Refer&Ground	Flickr30K Young et al. (2014)	Recall (IoU>0.5, any protocol)
	LVIS_Ferret Gupta et al. (2019); You et al. (2023)	Accuracy
	Refcoco Kazemzadeh et al. (2014)	Recall@1 (IoU>0.5)
	Refcoco+ Kazemzadeh et al. (2014)	Recall@1 (IoU>0.5)
	Refcocog Kazemzadeh et al. (2014)	Recall@1 (IoU>0.5)
	Ferret-Bench† You et al. (2023)	GPT-assisted score
Knowledge (Math/Science/Code)	AI2D Kembhavi et al. (2016b)	Accuracy
	ScienceQA Lu et al. (2022)	Accuracy-IMG
	MathVista Lu et al. (2023a)	GPT-assisted score
	MMMU Yue et al. (2023a)	Accuracy
Multi-image	Qbench2 Zhang et al. (2024e)	Accuracy
	Mantis Jiang et al. (2024)	Accuracy
	NLVR2 Suhr et al. (2018)	Accuracy
	BLINK Fu et al. (2024c)	Accuracy
	MVbench Li et al. (2023f)	Accuracy
	Muirbench† Wang et al. (2024)	Accuracy

- **Refer & ground Average Score**: average of the scores of Flickr30k, RefCOCO avg. and LVIS avg., where RefCOCO avg. is the average of RefCOCO A, RefCOCO B, RefCOCO+ A, RefCOCO+ B and RefCOCOg, and LVIS avg. is the average of point and box metrics.
- **Knowledge Average Score**: average score of the corresponding metric scores from AI2D, ScienceQA, MathVista and MMMU.
- **Multi-image average score**: average of Qbench, Mantis, NLVR2, BLINK and MVBench metric scores.
- **MMBaseScore**: average score of the *General Average Score*, *Text-rich Average Score* and *Knowledge Average Score*. This aggregated metric is used in Section 2 to measure the impact of the general, text-rich, and knowledge capabilities of a model.

A.5 Impact of Synthetic Captions by Self-Training

Besides using public captioning data mentioned in Section 2.3, we also follow (Fang et al., 2024) to study the effect of self-training using synthetic captions. This is particularly important because captioning data generated by black-box commercial models can sometimes be difficult to scale and data from open models, such as from the LLaVA-NeXT family may be constrained by these model's inherent limitations. We develop a self-augmented image-caption data engine building on our previous work, MM1 (McKinzie et al., 2024) with a goal to provide high quality captions in a computationally efficient manner. Specifically, we fine-tune a pre-trained 3B MM1-style model on a mix of synthetic and approximately 8k human-annotated paragraph-length image captions (approximately 70 tokens on average). We then apply this captioner at scale to 290 million web-crawled images with resolutions ranging from 512 to 1024px. Following the approach in (Liu et al., 2024a), we perform concept filtering based on the generated captions, resulting in a dataset of 7 million high-quality captions, which includes numerous text-rich examples and alt-text-derived knowledge.

Building on this, we investigate the impact of the volume of synthetic caption data. The synthetic captions, ranging from 1.4 million to 7 million, show consistent improvements in model performance across various metrics, as illustrated in Figure 9. Specifically, a ratio of 0 on the x-axis indicates that no image-caption data is added to the original OCR dataset, while ratios ranging from 0.2 to 1.0 on the x-axis represent the proportion of the total 7M dataset included in the training. For example, a ratio of 0.2 corresponds to approximately 1.4M image-caption pairs added with the original OCR data while 1.0 denotes all 7M are added into training.

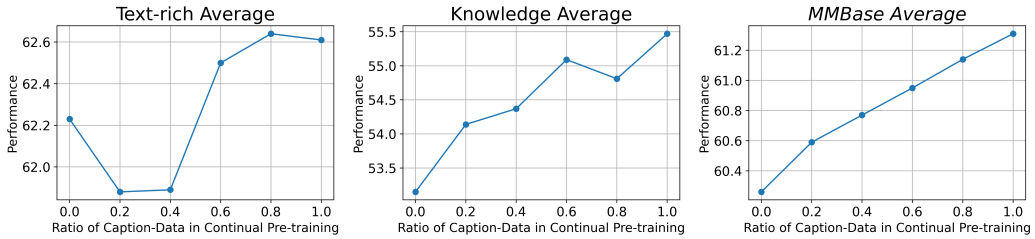

Figure 9: Impact of synthetic captions for continual pre-training the 3B model, building on top of the final MM1.5 strategy introduced in the main text, *i.e.*, including the OCR continual pre-training stage. We report the impact of adding incrementally more synthetic captions, up to 7M in total.

In contrast to the ShareGPT4V-PT and LLaVA-Recap-3M captions as explored in Section 2.3, we find that adding our in-house synthetic captions to the OCR data mixture can lead to consistent improvement for continual pre-training.[6] We observe improvements in knowledge-related benchmarks and the aggregated *MMBase* scores that further scale with increased data volume. This is especially notable since our in-house captioner uses only a 3B model while LLaVA-Recap, for example, uses a 34B model for captioning.

Our results suggest that while a comparatively simple OCR mixture represents a strong baseline for continual pre-training data, high-quality captions can still lead to further improvements. However, the quality, distribution, perhaps even style and length of the generated captions seem crucial to realize gains. While our in-house captions empirically outperformed publicly available data in our specific setting, further research is necessary as to what, specifically, these improvements are attributable to and whether further improvements can be achieved. This investigation goes beyond the scope of this paper, and we aim to study synthetic captioning further in future work.

A.6 Comparison with SOTA Models

We compared our model with selected benchmarks in Section 3. Here, we present comparisons with more baselines on extensive benchmarks in Table 7 (Knowledge & General), 8 (Text-rich), Table 9 (Refer & s Ground), Table 10 (In-context Learning), and Table 11 (Multi-image).

[6]Experiments in this section are based on the final recipe from Section 3, with slightly different settings compared to those in Section A.2.

Table 7: Comparison with SOTA models on knowledge and general benchmarks. (†) The score is the summation of perception and cognition scores. Gemini-1.5-Pro, GPT-4V and GPT-4o numbers are from OpenVLM Leaderboard.

Model	Knowledge Benchmarks				General Benchmarks					
	AI2D (test)	SQA (test)	MMMU (val)	MathV (testmini)	MME (P/C)	SEED^{I}	POPE	LLaVA^{W}	MM-Vet	RealWorldQA
1B Model Comparison										
LLaVAOneVision-0.5B Li et al. (2024c)	57.1	67.2	31.4	34.8	1238.0/240.0	65.5	–	–	29.1	55.6
SPHINX-Tiny Gao et al. (2024)	24.6	21.5	–	26.4	1261.2/242.1	–	82.2	52.3	23.8	–
DeepSeek-VL Lu et al. (2024)	–	–	32.2	31.1	–	–	87.6	–	34.8	–
TinyLLaVA Zhou et al. (2024)	–	60.1	–	–	–	–	86.1	60.8	25.8	–
Gemini Nano-1 Team et al. (2023)	37.9	–	26.3	27.3	–	–	–	–	–	–
IntenVL2-2B Chen et al. (2024b)	74.1	94.1	36.3	46.0	1864.3†	70.9	85.2	60.0	39.7	57.4
MM1-1B McKinzie et al. (2024)	57.7	62.3	33.2	31.1	1393.2/217.1	65.6	87.4	67.5	39.4	51.2
MM1.5-1B	59.3	82.1	35.8	37.2	1365.7/245.7	70.2	88.1	71.6	37.4	53.3
MM1.5-1B-MoE	67.1	87.6	41.2	42.9	1511.9/361.1	71.4	88.6	75.5	39.8	57.8
3B Model Comparison										
MiniCPM-V 2.0-3B Yao et al. (2024b)	62.9	80.7	38.2	38.7	1808.2†	67.1	87.8	69.2	38.2	55.8
VILA1.5-3B Lin et al. (2024b)	–	69.0	33.3	–	1442.4/–	67.9	85.9	–	–	–
TinyLLaVA Zhou et al. (2024)	–	69.1	–	–	1464.9/–	–	86.4	75.8	32.0	–
Gemini Nano-2 Team et al. (2023)	51.0	–	32.6	30.6	–	–	–	–	–	–
Bunny He et al. (2024)	–	78.3	41.4	–	1581.5/361.1	72.5	87.2	–	–	–
BLIP-3 Xue et al. (2024)	–	88.3	41.1	39.6	–	72.2	87.0	–	–	60.5
Phi-3-Vision-4B Abdin et al. (2024a)	76.7	90.8	40.4	44.5	1441.6/320.0	71.8	85.8	71.6	46.2	59.4
MM1-3B McKinzie et al. (2024)	62.4	69.4	33.9	32.0	1482.5/279.3	68.8	87.4	72.1	43.7	55.8
MM1.5-3B	65.7	85.8	37.1	44.4	1478.4/319.6	72.4	88.1	73.0	41.0	56.9
MM1.5-3B-MoE	69.9	89.8	42.9	46.9	1591.4/365.7	73.3	87.2	76.1	43.7	60.7
7B Model Comparison										
LLaVA-NeXT-7B Liu et al. (2024a)	–	70.1	35.8	34.6	1519.0/332.0	70.2	86.5	81.6	43.9	–
Idefics2-8B Laurençon et al. (2024a)	–	–	43.0	51.4	–	–	–	–	–	–
MM1-7B McKinzie et al. (2024)	66.0	72.6	37.0	35.9	1529.3/328.9	69.9	86.6	81.5	42.1	55.7
MM1.5-7B	72.2	89.6	41.8	47.6	1514.9/346.4	73.4	88.6	74.2	42.2	62.5
30B Model Comparison										
LLaVA-NeXT-34B Liu et al. (2024a)	–	81.8	51.1	46.5	1631.0/397.0	75.9	87.7	89.6	57.4	–
Cambrian-34B Tong et al. (2024a)	79.7	85.6	49.7	53.2	1689.3/–	75.3	–	–	–	67.8
MM1-30B McKinzie et al. (2024)	73.3	81.0	44.7	39.4	1637.6/431.4	72.1	87.6	89.3	48.7	59.4
MM1.5-30B	77.2	91.9	47.4	55.6	1646.2/405.7	75.0	88.6	80.4	52.0	69.0
Gemini-1.5-Pro Reid et al. (2024)	79.1	85.7	60.6	57.7	2110.6†	–	88.2	95.3	64.0	64.1
GPT-4V OpenAI (2024)	75.9	82.1	53.8	48.7	1771.5†	71.6	75.4	93.1	56.8	56.5
GPT-4o Islam & Moushi (2024)	84.6	90.7	69.2	61.3	2310.3†	77.1	85.6	102.0	69.1	75.4

Table 8: Comparison with SOTA models on text-rich benchmarks. Numbers marked with (†) are obtained from Li et al. (2024c).

Model	Text-rich Benchmarks						
	WTQ (test)	TabFact (test)	OCRBench (test)	ChartQA (test)	TextVQA (val)	DocVQA (test)	InfoVQA (test)
1B Model Comparison							
LLaVAOneVision-0.5B Li et al. (2024c)	–	–	–	61.4	–	70.0	41.8
SPHINX-Tiny Gao et al. (2024)	15.3	51.1	–	34.1	57.8	53.0	26.3
DeepSeek-VL Lu et al. (2024)	–	–	40.9	–	–	–	–
TinyLLaVA Zhou et al. (2024)	–	–	–	–	51.7	–	–
Gemini Nano-1 Team et al. (2023)	–	–	–	53.6	62.5	72.2	51.1
InternVL2-2B Chen et al. (2024b)	35.8	56.7	78.1	76.2	73.4	86.9	58.9
MM1-1B McKinzie et al. (2024)	19.9	49.8	56.6	61.8	68.2	68.4	38.5
MM1.5-1B	34.1	66.1	60.5	67.2	72.5	81.0	50.5
MM1.5-1B-MoE	38.9	71.4	62.6	73.7	76.1	84.8	55.9
3B Model Comparison							
MiniCPM-V 2.0-3B Yao et al. (2024b)	24.2	58.2	60.5	59.8	74.1	71.9	37.6
TinyLLaVA Zhou et al. (2024)	–	–	–	–	59.1	–	–
Gemini Nano-2 Team et al. (2023)	–	–	–	51.9	65.9	74.3	54.5
BLIP-3-4B Xue et al. (2024)	–	–	–	–	71.0	–	–
Phi-3-Vision-4B Abdin et al. (2024b)	47.4	67.8	63.7	81.4	70.1	83.3	49.0
MM1-3B McKinzie et al. (2024)	23.6	52.9	57.0	66.8	71.9	75.2	44.7
MM1.5-3B	41.8	72.9	65.7	74.2	76.5	87.7	58.5
MM1.5-3B-MoE	39.1	73.1	63.8	73.6	76.8	85.0	53.6
7B Model Comparison							
LLaVA-NeXT-7B Liu et al. (2024a)	–	–	–	–	64.9	–	–
Idefics2-8B Laurençon et al. (2024a)	–	–	–	–	73.0	74.0	–
DocOwl-1.5-Chat Hu et al. (2024a)	40.6	80.2	–	70.2	68.6	82.2	50.7
MM1-7B McKinzie et al. (2024)	28.8	55.5	62.6	72.6	72.80	76.8	45.5
MM1.5-7B	46.0	75.9	63.5	78.6	76.5	88.1	59.5
30B Model Comparison							
LLaVA-NeXT-34B Liu et al. (2024a)	–	–	–	–	69.5	–	–
Cambrian-34B Tong et al. (2024a)	–	–	60.0	75.6	76.7	75.5	–
MM1-30B McKinzie et al. (2024)	33.3	58.9	60.6	76.9	73.5	75.8	47.3
MM1.5-30B	54.1	84.0	65.8	83.6	79.2	91.4	67.3
Gemini-1.5-Pro Reid et al. (2024)	–	–	75.4	87.2	78.7	93.1	81.0
GPT-4V OpenAI (2024)	–	–	64.5	78.5†	–	88.4†	–
GPT-4o Islam & Moushi (2024)	–	–	73.6	85.7†	–	92.8†	–

Table 9: Comparison with SOTA models on referring and grounding benchmarks.

Model	Refer and Ground Benchmarks					
	RefCOCO (testA/B)	RefCOCO+ (testA/B)	RefCOCOg (test)	Flickr30k (test)	LVIS-Ref (box/point)	Ferret-Bench (avg.)
1B Model Comparison						
SPHINX-Tiny Gao et al. (2024)	86.9/77.9	78.5/63.7	78.9	–	–	–
MM1-1B McKinzie et al. (2024)	0/0	0/0	0	0	51.4/51.6	47.3
MM1.5-1B	89.3/81.9	83.7/69.3	82.8	83.0	69.7/54.7	67.4
MM1.5-1B-MoE	91.0/84.8	86.0/73.0	84.7	85.4	71.4/56.7	69.6
3B Model Comparison						
MiniCPM-v2-3B Yao et al. (2024b)	–	–	–	–	48.2/47.7	22.1
Phi-3-Vision-4B Abdin et al. (2024b)	46.3 / 36.1	42.0 / 28.8	37.6	27.12	53.8/54.5	32.2
InternVL2 Chen et al. (2024b)	88.2 / 75.9	82.8 / 63.3	78.3	51.6	51.0 / 51.1	35.0
MM1-3B McKinzie et al. (2024)	0/0	0/0	0	0	52.9/53.9	46.3
MM1.5-3B	92.0/86.1	87.7/75.9	86.4	85.9	76.3/59.5	69.5
MM1.5-3B-MoE	92.6/86.4	88.0/77.8	86.4	85.8	79.3/54.5	72.2
7B Model Comparison						
Qwen-VL-7B Bai et al. (2023)	92.3/84.5	88.6/76.8	86.3	–	–	–
MiniGPT-v2-7B Chen et al. (2023a)	91.3/84.3	85.5/73.3	84.3	–	–	–
LLaVA-OneVision-7B Abdin et al. (2024b)	80.0/61.6	76.9/56.2	70.0	50.1	51.2/51.4	38.4
Ferret-7B You et al. (2023)	91.4/82.5	87.4/73.1	84.8	82.2	79.4/67.9	64.5
Ferret-V2-7B Zhang et al. (2024a)	94.7/88.7	92.8/79.3	89.3	85.8	86.6/74.6	75.6
MM1-7B McKinzie et al. (2024)	0/0	0/0	0	0	53.1/53.3	48.5
MM1.5-7B	92.5/86.7	88.7/77.8	87.1	85.3	79.4/53.4	72.6
Larger (>13B) Model Comparison						
Ferret-13B You et al. (2023)	92.4/84.4	88.1/75.2	86.3	84.8	80.5/68.4	66.3
Ferret-V2-13B Zhang et al. (2024a)	95.0/88.9	92.8/81.4	90.0	86.3	87.7/75.1	74.9
MM1-30B McKinzie et al. (2024)	0/0	0/0	0	0	53.4/52.7	50.9
MM1.5-30B	94.9/89.5	92.4/83.5	90.0	87.5	84.9/61.4	77.1

Table 10: Comparison with SOTA models on VL-ICL benchmark Zong et al. (2024) for multimodal in-context learning. 4-shot accuracy reported for each subtask.

Model	VL-ICL Benchmark						
	CLEVR	Matching MiniImageNet	Open MiniImageNet	Operator induction	Operator induction interleaved	TextOCR	Avg.
1B Model Comparison							
MM1-1B McKinzie et al. (2024)	25.0	49.3	73.0	16.7	8.3	33.5	34.3
MM1.5-1B	39.0	52.0	84.0	60.0	36.7	34.0	51.0
MM1.5-1B-MoE	33.0	56.5	89.0	56.7	56.7	44.0	56.0
3B Model Comparison							
Phi-3-Vision-4B Abdin et al. (2024b)	17.0	50.0	1.0	26.7	8.3	14.0	19.5
MM1-3B McKinzie et al. (2024)	27.5	50.0	79.0	18.3	13.3	34.0	37.0
MM1.5-3B	33.5	59.0	88.0	48.3	66.7	42.5	56.3
MM1.5-3B-MoE	32.0	58.0	92.0	63.3	65.0	47.5	59.6
7B Model Comparison							
OpenFlamingo-9B Awadalla et al. (2023)	18.8	50.0	51.2	2.8	2.8	0.0	20.9
Idefics-9B Laurençon et al. (2024b)	27.7	50.0	53.8	7.8	6.1	22.8	28.0
Otter-9B Li et al. (2023a)	8.2	50.4	28.5	12.2	7.2	0.8	17.9
InternLM-XComposer2-7B Dong et al. (2024a)	20.0	50.1	49.0	39.4	11.1	16.0	30.9
Qwen-VL-Chat-7B Bai et al. (2023)	26.8	56.4	58.0	18.9	8.9	22.3	31.9
LLaVA-NeXT-7B Liu et al. (2024a)	17.8	50.0	0.0	3.3	5.0	0.0	12.7
MM1-7B McKinzie et al. (2024)	33.0	69.5	97.5	40.0	45.0	32.0	52.8
MM1.5-7B	25.5	52.8	98.5	68.3	60.0	31.0	56.0
Larger (>30B) Model Comparison							
Idefics-80B- Laurençon et al. (2024b)	31.5	50.0	52.5	21.7	28.3	29.5	35.6
Emu2-Chat-37B Sun et al. (2023a)	14.8	50.0	28.2	21.7	10.0	36.5	26.9
MM1-30B McKinzie et al. (2024)	25.0	63.0	98.5	51.7	38.3	36.0	52.1
MM1.5-30B	46.5	66.5	100.0	65.0	80.0	44.5	77.6
GPT-4V OpenAI (2024)	42.0	81.0	56.0	92.0	74.0	50.0	65.8

Table 11: Comparison with SOTA models on multi-image benchmarks. The result with mark (†) in the row of GPT-4V is from GPT-4o. MVBench Li et al. (2024h) is treated as a multi-image benchmark to test the zero-shot transfer capability of MM1.5 to video understanding tasks.

Model	Multi-image Benchmarks					
	QBench2 (val)	Mantis (test)	NLVR2 (val)	MVBench	BLINK (val)	Muirbench (test)
1B Model Comparison						
LLaVA-NeXT-Interleave-0.5B Li et al. (2024f)	52.0	45.6	67.8	45.6	39.2	–
LLaVAOneVision-0.5B Li et al. (2024c)	48.8	39.6	63.4	45.5	52.1	25.5
MM1-1B McKinzie et al. (2024)	43.4	41.5	50.9	43.8	40.3	30.7
MM1.5-1B	66.4	50.7	79.0	45.8	46.3	34.7
MM1.5-1B-MoE	70.9	51.2	83.2	48.3	43.7	40.9
3B Model Comparison						
BLIP-3-4B Xue et al. (2024)	75.1	56.7	–	–	49.7	–
Phi-3-Vision-4B Abdin et al. (2024b)	56.8	47.9	53.6	46.7	44.2	38.0
MM1-3B McKinzie et al. (2024)	41.4	45.2	51.7	44.8	41.5	28.0
MM1.5-3B	73.2	54.8	83.8	47.7	46.8	44.3
MM1.5-3B-MoE	73.8	54.4	86.0	50.3	49.8	45.6
7B Model Comparison						
LLaVA-v1.5-7B Liu et al. (2023a)	49.3	31.3	53.9	36.0	37.1	23.5
LLaVA-NeXT-Interleave-7B Li et al. (2024f)	74.2	62.7	88.8	53.1	52.6	38.9
Idefics2-8B Laurençon et al. (2024a)	57.0	48.9	86.9	29.7	45.2	26.1
Mantis-Idefics2-8B Jiang et al. (2024)	75.2	57.1	89.7	51.4	49.1	44.5
MM1-7B McKinzie et al. (2024)	43.6	51.6	59.9	45.3	40.0	30.4
MM1.5-7B	73.2	57.6	86.9	48.3	48.2	49.1
Larger (>14B) Model Comparison						
LLaVA-NeXT-Interleave-14B Li et al. (2024f)	76.7	66.4	91.1	54.9	52.1	–
Emu2-Chat-37B Sun et al. (2023a)	50.1	37.8	58.2	39.7	36.2	33.6
MM1-30B McKinzie et al. (2024)	42.8	52.5	63.1	47.1	43.5	36.7
MM1.5-30B	79.3	64.6	90.6	54.0	50.2	58.2
GPT-4V OpenAI (2024)	76.5	62.7	88.8	43.5	51.1	68.0†

A.7 MM1.5-VIDEO

The multi-image reasoning capability shown in MM1.5 naturally leads us to develop **MM1.5-Video** for video understanding. It takes a video and an instruction as input and generates the response. For the inputs, we uniformly sample N frames from the video at an arbitrary length and feed them into the model as multi-image inputs without special frame assembly. Due to the token limits, we disable the dynamic image splitting for each frame, and the vision encoder generates the feature maps frame-by-frame independently. Specifically, we sample 24 frames for each video, and each frame is represented by 144 tokens.

We introduce two variants for MM1.5-Video. First, we build MM1.5-Video as a *training-free* model, which is achieved by directly adopting the pre-trained MM1.5 image models to video tasks without being fine-tuned on any video data. This saves a lot of computation resources and demonstrates MM1.5's capability of transferring knowledge to new domains.

Second, we introduce the *supervised fine-tuning (SFT)* model where we fine-tune MM1.5 image models on video instruction-tuning datasets to improve its temporal modeling capability for video tasks. We use a mixture of public video datasets from ShareGPTVideo (Zhang et al., 2024c) (556K), VideoChat2 (Li et al., 2023e) (225K), and ActivityNet-QA (Yu et al., 2019) (31.5K). These datasets contain a variety of videos types, spanning different tasks (*e.g.,* open-ended and multiple choice questions), viewpoints (*e.g.,* first- and third-person views), and lengths (*e.g.,* videos from a few seconds to tens of minutes).

A.7.1 BENCHMARKS AND METRICS

We compare our video training-free and SFT models with state-of-the-art methods on multiple video question-answering (VideoQA) tasks and benchmarks.

Open-Ended Benchmarks evaluate the performance of a model to answer questions in a free-form style. For this task, we include ActivityNet-QA (Yu et al., 2019) and VCGBench (Maaz et al., 2024). Following prior work (Xu et al., 2024b), we use `GPT-3.5-Turbo-0125` to assess the accuracy and score for the prediction. Considering that the labeled answers of these two datasets are typically short (*e.g.,* one word or phrase), we also evaluate on the LLaVA-Hound (Zhang et al., 2024c), which requires the model to generate more detailed answers. This is useful for assessing performance on tasks involving detailed video understanding. We follow their original setting to report the score from `GPT-3.5-Turbo-0301` and consider a score value ≥ 3 as correct for accuracy calculation.

Multiple Choice Benchmarks require the model to pick the correct answer from multiple choices. For this evaluation, we include VideoMME (Fu et al., 2024b), EgoSchema (Mangalam et al., 2024), NExTQA (Xiao et al., 2021a), and IntentQA (Li et al., 2023c). VideoMME is a comprehensive evaluation dataset containing video from a few seconds to one hour in length. EgoSchema consists of egocentric videos and involves complex long-form temporal understanding and reasoning. NExTQA and IntentQA are collected from the same video source, but IntentQA focuses on predicting intents in daily social activities. For all these datasets, the accuracy of selecting the correct answer from the options is used as the evaluation metric.

A.7.2 RESULTS

Training-free results are shown in Table 12 and 13. MM1.5-Video demonstrates greater capability on Multiple Choice VideoQA, where MM1.5-Video-3B already outperforms state-of-the-art training-free 7B models on all benchmarks. We also find that MM1.5-Video can follow the instruction to precisely output the predicted option; however, most existing methods (Li et al., 2024h) use structured answer prompts (*e.g,* `"Best Option:("`) to guide their models to generate answers in a desirable format. On the other hand, MM1.5-Video achieves only on-par performance compared to SlowFast-LLaVA on the open-ended benchmarks. We hypothesize that this is because our multi-image SFT datasets contain primarily multiple choice tasks, making such a task formulation most similar to the training data.

SFT results are also shown in Table 12 and 13. First, we observe that fine-tuning MM1.5-Video on video datasets can improve its performance on all tasks. Second, on both open-ended and multiple choice benchmarks, our small model, MM1.5-Video-1B, significantly outperforms LLaVAOneVision-

Table 12: Comparison with SOTA models on Open-Ended and Multiple Choice benchmarks.

Model	Video Data	Open-Ended Benchmarks		Multiple Choice Benchmarks			
		ActivityNet-QA (test)	VCGBench (test)	VideoMME (w/o subs)	EgoSchema (subset)	NExTQA (val)	IntentQA (val)
Training-Free Model Comparison							
DeepStack-L-7B Meng et al. (2024)	✘	49.3	–	–	38.4	61.0	–
IG-VLM-7B (LLaVA-v1.6) Kim et al. (2024)	✘	54.3	3.03	–	35.8	63.1	60.3
SlowFast-LLaVA-7B Xu et al. (2024b)	✘	55.5	3.04	40.7	47.2	64.2	60.1
MM1.5-Video-1B (Training-free)	✘	46.8	2.86	45.6	45.4	70.0	67.8
MM1.5-Video-3B (Training-free)	✘	50.9	3.04	48.4	48.4	72.8	72.7
MM1.5-Video-7B (Training-free)	✘	52.5	3.05	52.4	49.6	76.1	76.7
SFT Model Comparison							
VideoChatGPT-7B Maaz et al. (2024)	✔	35.2	2.42	–	–	–	–
Video-LLaVA-7B Lin et al. (2023a)	✔	45.3	2.84	39.9	–	–	–
Vista-LLaMA-7B Ma et al. (2024)	✔	48.3	–	–	–	60.7	–
MovieChat+-7B Song et al. (2024)	✔	48.1	–	–	–	54.8	–
VideoChat2-7B Li et al. (2024h)	✔	49.1	2.98	–	–	68.6	81.9
Video-LLaMA2-7B Cheng et al. (2024)	✔	50.2	3.13	47.9	51.7	–	–
PLLaVA-7B Xu et al. (2024a)	✔	56.3	–	–	–	–	–
LLaVA-NeXT-Interleave-0.5B Li et al. (2024f)	✔	48.0	3.07	–	–	59.5	–
LLaVA-NeXT-Interleave-7B Li et al. (2024f)	✔	55.3	3.42	–	–	78.2	–
LLaVAOneVision-0.5B Li et al. (2024c)	✔	50.5	3.12	44.0	26.8	57.2	–
LLaVAOneVision-7B Li et al. (2024c)	✔	56.6	3.51	58.2	60.1	79.4	–
MM1.5-Video-1B (SFT)	✔	56.1	3.14	45.7	51.0	71.8	74.2
MM1.5-Video-3B (SFT)	✔	57.9	3.17	49.5	52.4	74.7	81.2
MM1.5-Video-7B (SFT)	✔	60.9	3.22	53.5	57.2	76.9	86.6

Table 13: Comparison with SOTA models on LLaVA-Hound benchmarks. (†) indicates the published version released at `https://huggingface.co/ShareGPTVideo/LLaVA-Hound-SFT`.

Model	In-domain Benchmarks			Out-of-domain Benchmarks			
	ActivityNet-QA	VIDAL-QA	WebVid-QA	MSVD-QA	MSRVTT-QA	TGIF-QA	SSV2-QA
Video-ChatGPT-7B Maaz et al. (2024)	34.2	29.4	38.9	34.1	25.7	31.4	19.4
LLaMA-VID-7B Li et al. (2023g)	36.5	30.6	37.0	34.1	25.0	27.2	22.2
Chat-UniVi-7B Jin et al. (2024a)	39.4	31.4	40.1	35.6	25.9	33.2	20.6
Video-LLaVA-7B Lin et al. (2023a)	41.4	34.3	42.5	39.5	30.8	33.0	24.3
LLAVA-HOUND-SFT-7B†	62.8	56.3	66.8	62.2	52.6	61.1	35.4
MM1.5-Video-1B (Training-free)	49.0	42.6	55.8	49.8	43.3	47.6	27.2
MM1.5-Video-3B (Training-free)	51.5	45.4	58.5	51.1	46.0	49.2	28.2
MM1.5-Video-7B (Training-free)	52.8	48.7	58.5	52.9	48.1	49.8	30.4
MM1.5-Video-1B (SFT)	65.7	60.6	68.7	65.0	55.3	64.0	34.0
MM1.5-Video-3B (SFT)	67.8	63.4	71.1	65.2	57.2	64.9	35.2
MM1.5-Video-7B (SFT)	68.5	68.5	71.5	67.2	59.3	65.5	37.9

0.5B (*e.g.,* 24.2% on EgoSchema and 14.6% on NExTQA) and achieves the state-of-the-art results. Third, our 7B model achieves state-of-the-art performance on ActivityNet-QA (*e.g.,* outperforming LLaVAOneVision-7B by 4.3%) and very strong results (mostly runner-up) on other benchmarks by using only public video datasets. We are impressed by the superior results of LLaVAOneVision-7B, especially on long-form video benchmarks such as VideoMME and EgoSchema. We hypothesize this can be due to that (i) it is trained on their re-annotated video datasets with better labeling quality, (ii) it takes more video frames as inputs (*i.e.,* 32 vs. 24), (iii) it uses multiple training stages on joint image and video datasets. We will explore these directions to improve our model in future work. Lastly, MM1.5-Video achieves state-of-the-art performance on the LLaVA-Hound benchmarks, which demonstrates our capability for detailed video understanding.

A.8 MM1.5-UI

One of the most promising applications of MLLMs that has recently gained popularity is using them to understand and act on user interfaces (UIs) on behalf or alongside users (Hong et al., 2024b; Baechler et al., 2024; You et al., 2024; Li & Li, 2023), which could significantly boost users' productivity and efficiency when interacting with digital devices. This application typically involves providing a model input of: (i) an image of the graphical user interface (GUI) of a device (*i.e.*, phone or computer) screen; and (ii) instructions on either knowledge *grounded* on certain areas or the entirety of the screen (*e.g.*, Is this element at <x1,x2,y1,y2> clickable?), or asking it to *refer* to certain areas of the screen that fit the questions' criterion (*e.g.*, Where is the text 'login' on the screen?). Beyond referring and grounding abilities, excelling on UI tasks also requires text-rich image understanding ability to

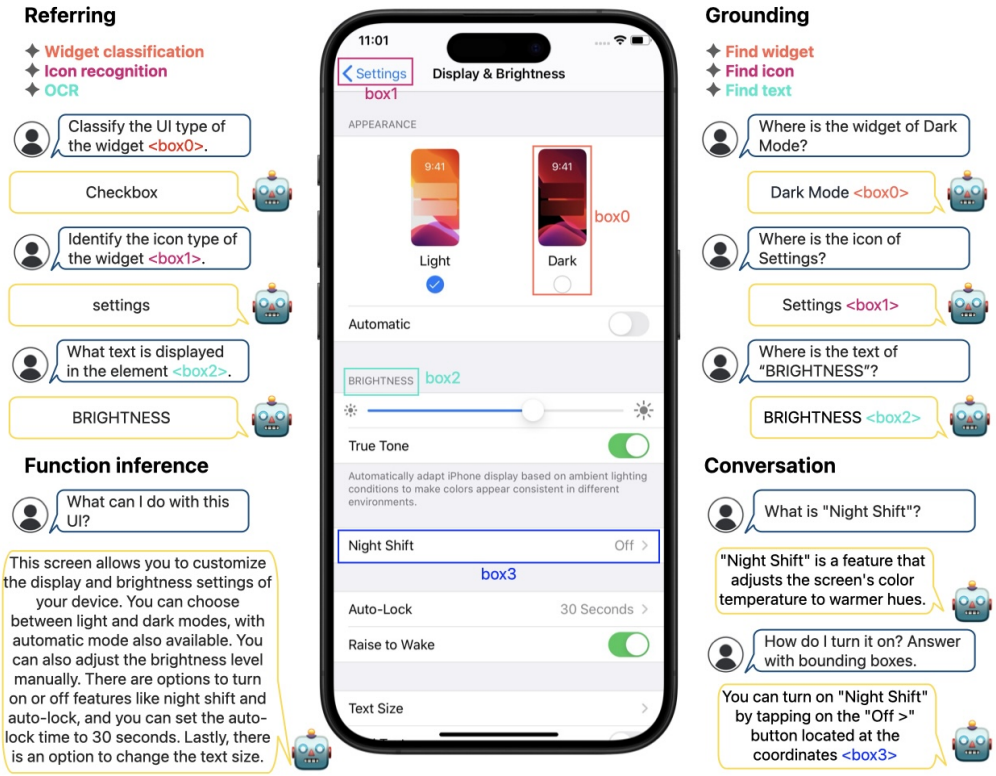

Figure 10: Illustration of the UI understanding capability shown in MM1.5-UI. Our single model is able to perform a variety of referring and grounding tasks and establish new state-of-the-arts. Moreover, it can summarize the functions of the UI screen and engage with users through conversations.

understand text-dense UIs, and background knowledge about typical user interactions on devices, which makes MM1.5 a perfect candidate to be developed into a highly capable UI understanding model.

Towards this goal, we developed **MM1.5-UI**, an MM1.5 model variant further fine-tuned specifically on UI data that achieves competitive performance on UI understanding tasks and establishes new state-of-the-art performance in various benchmarks. Figure 10 illustrates a single MM1.5-UI model's wide range of UI understanding capabilities on an iPhone screenshot. The model can find certain text ("BRIGHTNESS") on the left side (box2), correctly identify the settings icon at the top left (box1), classify a UI element on the right as a checkbox (box0), and maintain a multi-turn conversation about the "Night Shift" function (box3) in the UI.

A.8.1 Benchmarks and Metrics

We train and evaluate MM1.5-UI on a variety of public and elementary UI understanding tasks used in Ferret-UI (You et al., 2024). These tasks are established benchmarks in literature that cover multiple aspects of UI understanding, and allow us to fairly compare MM1.5-UI against prior work:

- **Public Benchmarks** include screen2words (Wang et al., 2021): a screen-level captioning task; widget captions (Li et al., 2020): a widget-level captioning task; and taperception (Schoop et al., 2022): predicting the tapability of a certain widget on the UI.
- **Ferret-UI** elementary tasks are split into two categories: Grounding (Grd-*) are questions querying for a certain area on the screen, such as finding an icon; and Referring (Ref-*) are questions given a certain area on the screen, such as recognizing text within a screen area (*i.e.*, OCR). Each of these tasks also has an iOS (*-i) and Android (*-A) version, forming four categories of tasks (*e.g.*, Grounding task on Android is Grd-A).

Table 14: Comparison with SOTA models on UI benchmarks. S2W: screen2words, WiC: widget captioning, TaP: taperception. (†) denotes per-task fine-tuning. 1 ep. means 1 epoch model training.

Model	Public Benchmarks			Ferret-UI Elementary Tasks			
	S2W	WiC	TaP	Ref-i	Ref-A	Grd-i	Grd-A
Spotlight Li & Li (2023)	106.7	141.8	88.4	-	-	-	-
PaliGemma-3B† Beyer et al. (2024)	119.6	148.4	-	-	-	-	-
Ferret-UI-13B You et al. (2024)	113.4	142.0	78.4	80.5	82.4	79.4	83.5
MM1.5-UI-1B	103.0	144.4	79.3	90.0	88.6	86.5	88.2
MM1.5-UI-3B	103.3	145.0	80.4	90.8	89.2	87.3	88.8
MM1.5-UI-7B	100.6	149.7	80.3	91.2	89.2	87.2	88.6
MM1.5-UI-30B	106.0	145.9	80.6	91.8	89.7	88.2	89.1
Ablation on MM1.5 SFT on UI tasks							
MM1.5-UI-3B (1 ep.)	103.9	145.2	77.4	88.6	87.7	86.0	87.9
MM1.5-UI-3B (1 ep., w/o MM1.5 SFT)	103.8	139.5	75.3	88.2	87.4	85.5	87.1

More details of the benchmarks can be found in Appendix A.10 and the original Ferret-UI paper (You et al., 2024).

A.8.2 Results

MM1.5-UI models are trained by further fine-tuning the final MM1.5 models on the Ferret-UI data mixture (You et al., 2024), which includes training data corresponding to the above elementary UI tasks and additional GPT-4-generated conversations about functionalities and descriptions about the UIs' functionality and layouts. There are 801K samples in total. All models are trained with the same batch size and learning rate as the original MM1.5 model.

Comparison with Prior Art. Results are summarized in Table 14. Our MM1.5-UI models outperform prior best models in nearly all benchmarks except Screen2words. In particular, even our 1B model is able to outperform the Ferret-UI model in its proposed elementary tasks by a wide margin despite being ten times smaller. The performance difference is most significant on iOS tasks at 9.1 points on average. This demonstrates that the abilities learned by MM1.5 are relevant and useful for UI tasks.

When comparing the performance across individual benchmarks, MM1.5-UI demonstrates a clear hierarchy of difficulties among tasks that focus on different types of UI elements, similar to Ferret-UI (You et al., 2024). Tasks focused on text are the most challenging, followed by those involving icons, while widget-based tasks are the easiest. This trend holds for both referring and grounding tasks. However, MM1.5-UI shows a notable performance improvement in icon-based tasks, significantly narrowing the gap between icon and widget tasks. Ferret-UI highlighted the importance of resolution for tasks involving smaller elements like icons. The higher resolution and dynamic image splitting used in MM1.5-UI further confirm that resolution is particularly beneficial for enhancing performance in icon-related tasks.

Impact of MM1.5 SFT on UI tasks. To highlight the effectiveness of the MM1.5 SFT mixture on downstream UI tasks (*i.e.*, in MM1.5-UI), we compare the performance of the full MM1.5-UI model with a baseline UI model fine-tuned with UI data on the pre-training checkpoint that MM1.5 was trained on. Both models are trained for one epoch using the Ferret-UI dataset, and their results are presented in Table 14. The final MM1.5-UI model, which underwent SFT for general domain, text-rich, and refer&ground tasks, achieves superior UI performance within the same number of training steps. This demonstrates the strong transfer capability of MM1.5 for UI applications and contributes to its performance improvement over prior SOTA models.

Impact of model scaling. We observe overall performance improvements as models scale, though gains in all metrics remain modest, suggesting that larger models may be constrained by factors such as data diversity, image resolution, or overfitting. For instance, in the most challenging OCR tasks, 47.8% of incorrect responses contain the ground truth as a strict substring of the generated response, or vice versa. This suggests the model accurately recognized the text but failed to trim or include the correct amount. Additionally, the performance of the 7B and 30B models appears to have plateaued,

indicating that larger, more diverse datasets and joint SFT of UI and core capabilities could further improve the performance.

A.9 MM1.5 In-House Multi-Image SFT Data

We generated two sets of in-house SFT data for the multi-image capabilities of our model: coco-instruct-interleaved and icl-instruct.

Coco-instruct-interleaved was generated using an LLaVa-style approach using our text-only LLM. We input COCO image captions for two images, along with a prompt requiring the LLM to generate a conversation between a user and an assistant, with the two images inserted in context. This dataset helps our model learn conversational multi-image capabilities. An example from this dataset is shown below. This dataset contains ~2k examples, with 2 images per example.

> **User**: <image 1> What do you see in the following picture?
> **Assistant**: I see an open beige toilet with a monitoring device attached to the seat. The device appears to be displaying various metrics, such as temperature and pressure, and it is likely used for medical purposes.
> **User**: <image 2> What about this picture?
> **Assistant**: I see a row of parking meters sitting next to each other near a street. The meters are typical of those used to enforce parking regulations in many cities.
> **User**: What is the difference between the two pictures?
> **Assistant**: The first picture depicts a toilet with a monitoring device, while the second picture shows a row of parking meters. These are two very different objects in different settings. The first picture is likely used for medical purposes, while the second picture is used to regulate parking in cities.

Icl-instruct was generated manually to help the model retain in-context learning abilities from pre-training along with more nuanced in-context learning tasks that require multi-step reasoning from the model. This dataset contains different varieties of in-context learning tasks, some of which are similar to those found in the VL-ICL benchmark (Zong et al., 2024). We found that including this dataset, which contains ~500 examples, greatly boosts the models' in-context learning performance.

A.10 MM1.5-UI Benchmark Details

The public benchmark tasks and metrics for evaluating MM1.5-UI are:

- **Screen2words** is a captioning task where each complete screen is paired with 5 ground-truth high-level summaries under ten words. The generated summaries' quality is measured by CIDEr score between the ground-truth and generated summaries.
- **Widget Captioning** is a captioning task where a certain screen area that corresponds to a widget (*e.g.*, button, list item) is paired with 3 ground-truth captions. The generated summaries' quality is measured by CIDEr score similar to Screen2words.
- **Taperception** is a binary classification task where a certain screen area that correspond to a widget (*e.g.*, button, list item) is paired with a ground-truth binary label of whether the screen area is 'tappable' (*i.e.*, clickable by users). The generated labels' quality is measured by F1 score.

The Ferret-UI Elementary task benchmarks used to evaluate MM1.5-UI, organized by capability categories, are:

- **Ferret-UI Grounding (Grd-i/A)** is a set of three grounding-based UI tasks introduced in Ferret-UI (You et al., 2024). These tasks query for certain areas of screens that meet certain criteria. They include finding a widget given a text description, finding an icon given the class of the icon, and finding a text location on screen. The expected response from the model is a bounding box, and the quality of the bounding box is measured by Recall with IoU>0.5.
- **Ferret-UI Referring (Ref-i/A)** is a set of three referring-based UI tasks introduced in Ferret-UI (You et al., 2024). These tasks query about knowledge or characteristics that correspond to certain areas of the screens. They include classifying the type of widgets in the given areas, recognizing the type of icons in the given areas, and recognizing texts in the given areas. The quality of the responses is measured by exact match accuracies.

Figure 11: Illustration of image grid selection used in dynamic image splitting for high-resolution image encoding. (Left) If the grid can cover the full image without scaling down, we choose the grid that minimizes padding. (Right) Otherwise, we choose the grid that minimizes the resolution loss due to scaling down.

Each of these two sets Ferret-UI tasks further have two variants with screenshots from two types of operating systems (iOS/Android), of which Android tasks are denoted as -A (*e.g.*, Grd-A), and iPhone tasks as -i, which results in 12 tasks in total.

A.11 Dynamic vs Static Image Splitting

Detailed ablation study of MM1.5 with different image splitting strategies is shown in Table 15, 16, 17 and 18. All models are using the final setting except for the image splitting (dynamic vs. static).

Table 15: Comparison of our models when using dynamic vs. static image splitting. We follow our final settings for all models. (S) and (D) indicate static and dynamic splitting, respectively.

Model	Knowledge Benchmarks				General Benchmarks					
	AI2D (test)	SQA (test)	MMMU (val)	MathV (testmini)	MME (P/C)	$SEED^{I}$	POPE	$LLaVA^{W}$	MM-Vet	RealWorldQA
1B Model Comparison										
MM1.5-1B(S)	59.5	83.9	36.1	37.4	1393.4/244.9	69.99	87.9	67.9	34.2	51.8
MM1.5-1B(D)	59.3	82.1	35.8	37.2	1365.7/245.7	70.2	88.1	71.6	37.4	53.3
MM1.5-1B-MoE(S)	66.4	86.8	41.2	42.2	1481.4/293.6	71.3	89.5	76.5	41.8	60.1
MM1.5-1B-MoE(D)	67.1	87.6	41.2	42.9	1511.9/361.1	71.4	88.6	75.5	39.8	57.8
3B Model Comparison										
MM1.5-3B(S)	66.1	87.2	36.8	43.1	1439.8/297.5	71.9	88.3	72.1	38.3	58.8
MM1.5-3B(D)	65.7	85.8	37.1	44.4	1478.4/319.6	72.4	88.1	73.0	41.0	56.9
MM1.5-3B-MoE(S)	66.3	89.3	41.9	43.1	1527.8/342.5	72.4	88.4	78.5	41.4	59.2
MM1.5-3B-MoE(D)	69.9	89.8	42.9	46.9	1591.4/365.7	73.3	87.2	76.1	43.7	60.7
7B Model Comparison										
MM1.5-7B(S)	72.2	89.6	44.1	49.1	1531.3/366.4	73.5	88.6	77.2	43.3	57.0
MM1.5-7B(D)	72.2	89.6	41.8	47.6	1514.9/346.4	73.4	88.6	74.2	42.2	62.5
30B Model Comparison										
MM1.5-30B(S)	75.4	92.8	46.8	56.0	1605.2/402.1	74.1	89.0	79.5	49.4	68.0
MM1.5-30B(D)	77.2	91.9	47.4	55.6	1646.2/405.7	75.0	88.6	80.4	52.0	69.0

A.12 Methodology for Running Competitor Models

This section covers the methodology used to report results for Phi-3-Vision (Abdin et al., 2024b), LLaVA-OneVision (Li et al., 2024c), InternVL2 (Chen et al., 2024b) and MiniCPM-V2 (Yao et al., 2024b). When available, we reported the results published by the original authors, either in their technical reports or on public leaderboards[7]. When not available, we implemented inference runners using publicly released checkpoints. Commonly, we followed (Li et al., 2024b)'s implementations that we adapted on our own internal fork of lm-eval-harness (Gao et al., 2023; McKinzie et al., 2024). To verify the validity of our inference implementations, we ensured we could reproduce previously published results within standard deviation. Below, we share details for each model implementation:

[7] `https://huggingface.co/spaces/opencompass/open_vlm_leaderboard`

Table 16: Comparison of our models when using dynamic vs. static image splitting. We follow our final settings for all models. (S) and (D) indicate static and dynamic splitting, respectively.

Model	Text-rich Benchmarks						
	WTQ (test)	TabFact (test)	OCRBench (test)	ChartQA (test)	TextVQA (val)	DocVQA (test)	InfoVQA (test)
1B Model Comparison							
MM1.5-1B(S)	31.0	65.4	60.4	67.5	72.8	79.7	40.8
MM1.5-1B(D)	34.1	66.1	60.5	67.2	72.5	81.0	50.5
MM1.5-1B-MoE(S)	34.1	69.6	58.0	72.7	75.8	82.5	46.0
MM1.5-1B-MoE(D)	38.9	71.4	62.6	73.7	76.1	84.8	55.9
3B Model Comparison							
MM1.5-3B(S)	36.3	71.0	61.1	74.3	75.2	84.0	45.8
MM1.5-3B(D)	41.8	72.9	65.7	74.2	76.5	87.7	58.5
MM1.5-3B-MoE(S)	32.5	70.1	60.2	73.0	75.9	81.0	44.2
MM1.5-3B-MoE(D)	39.1	73.1	63.8	73.6	76.8	85.0	53.6
7B Model Comparison							
MM1.5-7B(S)	38.4	73.7	59.7	77.9	76.1	84.5	47.3
MM1.5-7B(D)	46.0	75.9	63.5	78.6	76.5	88.1	59.5
30B Model Comparison							
MM1.5-30B(S)	46.0	81.0	64.5	82.4	78.7	88.5	53.2
MM1.5-30B(D)	54.1	84.0	65.8	83.6	79.2	91.4	67.3

Table 17: Comparison of our models when using dynamic vs. static image splitting. We follow our final settings for all models. (S) and (D) indicate static and dynamic splitting, respectively.

Model	Refer and Ground Benchmarks			
	RefCOCO avg.	Flickr30k (test)	LVIS avg.	Ferret-Bench avg.
1B Model Comparison				
MM1.5-1B(S)	82.0	82.7	62.4	69.7
MM1.5-1B(D)	81.4	83.0	62.2	67.4
MM1.5-1B-MoE(S)	79.3	80.9	63.9	73.4
MM1.5-1B-MoE(D)	84.8	85.4	64.6	69.6
3B Model Comparison				
MM1.5-3B(S)	85.1	85.3	68.1	71.2
MM1.5-3B(D)	85.6	85.9	67.9	69.5
MM1.5-3B-MoE(S)	82.8	82.6	67.5	70.8
MM1.5-3B-MoE(D)	86.2	85.8	66.9	72.2
7B Model Comparison				
MM1.5-7B(S)	87.2	86.0	68.8	71.2
MM1.5-7B(D)	86.6	85.3	66.4	72.6
30B Model Comparison				
MM1.5-30B(S)	90.1	87.7	73.2	75.6
MM1.5-30B(D)	90.1	87.5	73.1	77.1

Phi-3-Vision. We used the public Phi-3-Vision checkpoint[8] and ran it on our families of benchmarks. For **general**, **text-rich**, **knowledge** and **refer&ground** benchmarks, when the position of the image is not determined by the task, we prepend the image to the text input following the examples given in the Phi-3-Vision cook book[9]. For **grounding** benchmarks, we introduced the following prompt: "Question: {question}<b>Answer this question by listing the requested entities and their bounding boxes. The bounding boxes are formatted as follows: <x1,y1,x2,y2>, each value is between 0-{upper_bound}.<n>Answer:". For both **referring** and **grounding**, we experimented with a variety of upper bound bounding boxes. Through our experiments, we noticed that an upper box of 1 yielded to

[8] `https://huggingface.co/microsoft/Phi-3-vision-128k-instruct`

[9] https://github.com/microsoft/Phi-3CookBook/blob/main/md/03.Inference/Vision_Inference.md#3-comparison-of-multiple-images

Table 18: Comparison of our models when using dynamic vs. static image splitting. We follow our final settings for all models. (S) and (D) indicate static and dynamic splitting, respectively.

Model	Multi-image Benchmarks					
	QBench2 (val)	Mantis (test)	NLVR2 (val)	MVBench	BLINK (val)	Muirbench (test)
1B Model Comparison						
MM1.5-1B(S)	65.8	48.4	78.6	46.1	41.9	34.0
MM1.5-1B(D)	66.4	50.7	79.0	45.8	46.3	34.7
MM1.5-1B-MoE(S)	70.2	52.1	83.0	47.4	44.8	42.5
MM1.5-1B-MoE(D)	70.9	51.2	83.2	48.3	43.7	40.9
3B Model Comparison						
MM1.5-3B(S)	72.0	53.5	83.9	47.8	42.5	44.5
MM1.5-3B(D)	73.2	54.8	83.8	47.7	46.8	44.3
MM1.5-3B-MoE(S)	70.4	54.4	85.3	47.2	47.1	44.2
MM1.5-3B-MoE(D)	73.8	54.4	86.0	50.3	49.8	45.6
7B Model Comparison						
MM1.5-7B(S)	73.0	56.7	87.2	49.7	47.6	53.8
MM1.5-7B(D)	73.2	57.6	86.9	48.3	48.2	49.1
30B Model Comparison						
MM1.5-30B(S)	77.0	64.5	90.2	49.9	48.4	60.1
MM1.5-30B(D)	79.3	64.6	90.6	54.0	50.2	58.2

better results, in line with the answers produced by Phi-3-Vision. For Flickr30k, we slightly simplified the benchmark and asked the model to ground one entity per prompt, as grounding multiple entities jointly did not lead to satisfactory results.

LLaVA-OneVision. We used the public checkpoint LLaVA-OneVision 7B[10] and we followed closely the LLaVA documentation[11]. When not baked directly into the benchmarks, we used the original LlaVA prompts specified in (Liu et al., 2023a; Li et al., 2024c) for all families of benchmarks. In particular, for **grounding** benchmarks, we used the prompt introduced in Table 18 of (Li et al., 2024c): "Provide the bounding box coordinate of the region this sentence describes". On Flickr30k, we followed the single-entity approach outlined above.

InternVL2. The InternVL2 authors provided already a comprehensive set of benchmarks on **general**, **text-rich**, **knowledge** and **refer&ground** families[12], which we reported first. For the few remaining benchmarks, we used the 2B public checkpoint released. InternVL2 code base relies on both VLMEvalKit (Duan et al., 2024) and a custom internal evaluation[13]. We carefully reviewed the logic implemented[14], especially regarding the decoding parameters and prompts used. For **grounding**, we used the prompt shared by the authors: "Please provide the bounding box coordinates of the region this sentence describes: <ref>{question}</ref>". On Flickr30k, we followed the single-entity approach outlined above.

MiniCPM-V2. We used the publicly released MiniCPM-V2 2.8B checkpoint[15]. Similarly to InternVL2, MiniCPM-V2 code base relies on both VLMEvalKit and a custom internal implementation[16], which we reviewed carefully to reproduce decoding parameters and prompts. For **refer&ground** benchmarks, we noticed that regardless of the prompt used, MiniCPM-V2 could not produce satisfac-

[10] https://huggingface.co/lmms-lab/llava-onevision-qwen2-7b-ov

[11] https://github.com/LLaVA-VL/LLaVA-NeXT/blob/main/docs/LLaVA_OneVision_Tutorials.ipynb

[12] https://huggingface.co/OpenGVLab/InternVL2-2B

[13] https://internvl.readthedocs.io/en/latest/internvl2.0/evaluation.html

[14] https://github.com/OpenGVLab/InternVL

[15] https://huggingface.co/openbmb/MiniCPM-V-2

[16] https://github.com/OpenBMB/MiniCPM-V/tree/main/eval_mm

tory results on RefCOCO and Flickr30k[17]. We decided not to include those results. For **multi-image** and **in-context learning** benchmarks, we found that MiniCPM-V2 does not accept multiple images as input in its Hugging Face implementation. We acknowledge MiniCPM-V2's authors used a custom image concatenating approach for BLINK[18], but we could not reproduce easily the same approach on other benchmarks. We decided to only include the BLINK score reported by the authors[19].

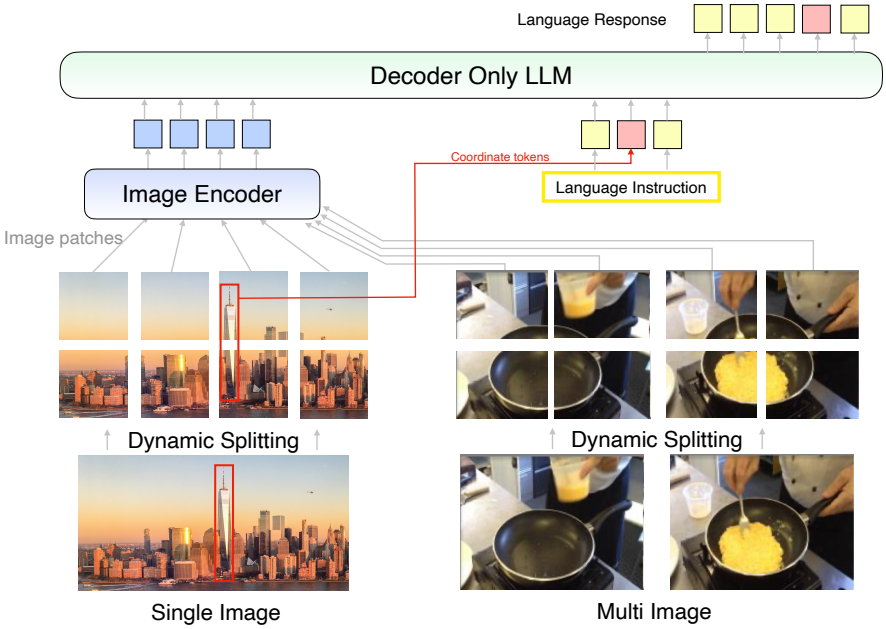

Figure 12: The overview of model architecture. MM1.5 excels at (i) text-rich image understanding with dynamic image splitting, (ii) visual referring and grounding with coordinate tokens, and (iii) multi-image reasoning.

[17]Responses commonly produced incomplete bounding boxes, preventing any parsing for a fair evaluation.

[18]https://github.com/OpenBMB/MiniCPM-V/blob/a209258d851f404485e5ae25864417dff3bb74ca/eval_mm/vlmevalkit/vlmeval/api/base.py#L260

[19]https://huggingface.co/spaces/opencompass/open_vlm_leaderboard

A.13 Qualitative Examples

A.13.1 MM1.5 Capabilities

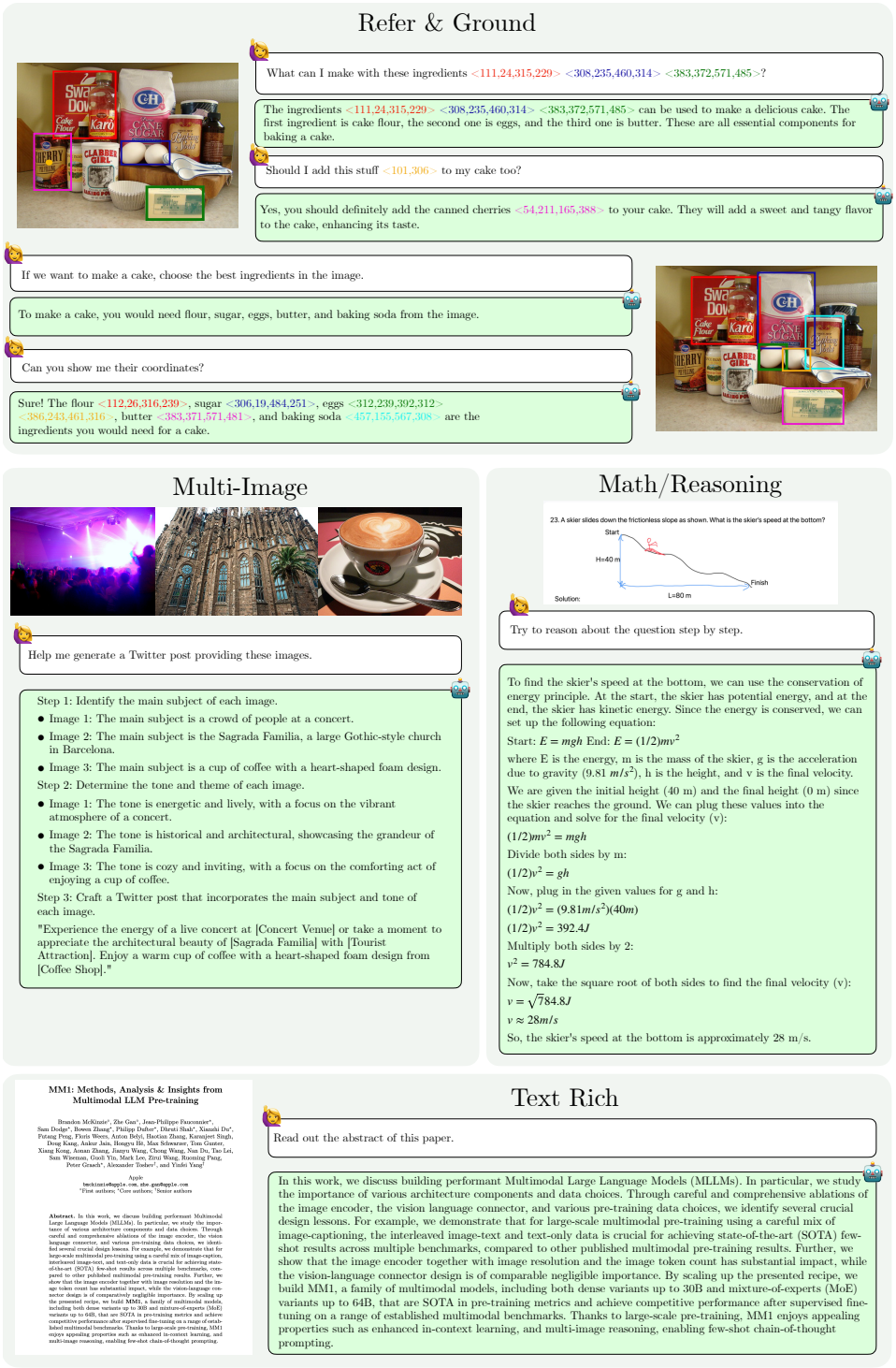

Figure 13: Examples of MM1.5 capabilities. The examples we demonstrated are generated by the MM1.5-3B model..

A.13.2 TEXT-RICH IMAGE UNDERSTANDING

The New York Times.

ARMISTICE SIGNED, END OF THE WAR! BERLIN SEIZED BY REVOLUTIONISTS; NEW CHANCELLOR BEGS FOR ORDER; OUSTED KAISER FLEES TO HOLLAND

Could you summarize every article on this newspaper page?

The newspaper page is from The New York Times dated November 11, 1918. The main headline announces the signing of the Armistice, marking the end of World War I. Other articles cover the revolution in Germany, with Berlin being seized by revolutionists and the abdication of Kaiser Wilhelm II. The page also includes a call for the abdication of the German Emperor by the socialist Chancellor, Friedrich Ebert. Additionally, there are reports on the ousting of Kaiser Wilhelm II and his flight to the Netherlands, as well as the resignation of the German General Staff. The page also features a report on the armistice being signed in France, marking the end of the war.

THE GUARDIAN

CONSCIENCE, NURTURED BY TRUTH On Saturday

AUGUST 8, 1998 FIFTY NAIRA

60 die in blasts at US embassies

Clinton condoles victims' families

Ojukwu forecloses presidential ambition

SPECIAL SALES !!

Samsonite/Carlton luggage

All brand of generators

High quality crystals /glasswares

Special discount on all TVs

MEGA PLAZA — You can't get a better deal anywhere!!

Could you summarize the articles in this newspaper page?

The newspaper page features several articles. The main headline reports on the tragic event of 60 people dying in blasts at US embassies. Another article discusses President Clinton consoling the victims' families. There's also a piece about Ojukwu foreclosing on a presidential ambition. Additionally, the page includes a special sales advertisement for Samsonite/Carlton luggage and high-quality crystals.

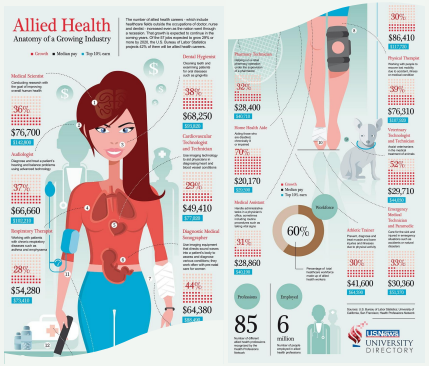

What percent of growth is expected in the primary technician jobs in the U.S.?

32%

How much is the top 10% income earned by medical assistants in the U.S.?

$40,190

What is the expected growth rate of physical therapist jobs in the U.S.?

39%

Title	Sales	Series	Platform(s)	Initial release date
Minecraft	300,000,000	*Minecraft*	Multi-platform	November 18, 2011[c]
Grand Theft Auto V	200,000,000	*Grand Theft Auto*	Multi-platform	September 17, 2013
Wii Sports	82,900,000	*Wii*	Wii	November 19, 2006
PUBG: Battlegrounds	75,000,000	*PUBG Universe*	Multi-platform	December 20, 2017
Mario Kart 8 / Deluxe	71,360,000	*Mario Kart*	Wii U / Switch	May 29, 2014
Red Dead Redemption 2	65,000,000	*Red Dead*	Multi-platform	October 26, 2018
Terraria	58,700,000	None	Multi-platform	May 16, 2011
Super Mario Bros.	58,000,000	*Super Mario*	Multi-platform	September 13, 1985
Overwatch		*Overwatch*	Multi-platform	May 24, 2016
Human: Fall Flat	50,000,000	None	Multi-platform	July 22, 2016
The Witcher 3: Wild Hunt		*The Witcher*	Multi-platform	May 19, 2015
Tetris (Game Boy / NES)	48,000,000	*Tetris*	Game Boy / NES	June 14, 1989
Pokémon Red / Green / Blue / Yellow	47,520,000	*Pokémon*	Multi-platform	February 27, 1996
Animal Crossing: New Horizons	45,850,000	*Animal Crossing*	Nintendo Switch	March 20, 2020
Wii Fit / Plus	43,800,000	*Wii*	Wii	December 1, 2007
Pac-Man	42,000,000	*Pac-Man*	Multi-platform	May 22, 1980

Can you give me a table of games and sales numbers, but only show games released before 2010

Sure, here is a table of games released before 2010 and their sales numbers:

Title	Sales	Series	Platform(s)	Initial release date
Wii Sports	82,900,000	Wii	Wii	November 19, 2006
Super Mario Bros.	58,000,000	Super Mario	Multi-platform	September 13, 1985
Tetris (Game Boy / NES)	48,000,000	Tetris	Game Boy / NES	June 14, 1989
Pokémon Red / Green / Blue	47,520,000	Pokémon	Multi-platform	February 27, 1996
Pac-Man	42,000,000	Pac-Man	Multi-platform	May 22, 1980

A.13.3 VISUAL REFERRING AND GROUNDING

Show me the guidelines for selecting the Ripe and Sweet melon

Uniform Size & Heavy: Pick a watermelon that is uniform in size and feels heavy for its size. This indicates that it is full of juice.

Larger "Webbing": Choose a watermelon with larger webbing, as it is likely to be sweeter.

Dark & Dull: A ripe watermelon will have a dark and dull exterior, which means it's ready to be enjoyed.

Field Spot: Look for a watermelon with a field spot, which is a yellow or orange spot on the bottom where it was resting on the ground. This indicates that it was allowed to ripen on the vine.

Orange Field Spot: The ideal watermelon will have an orange field spot, which means it was harvested at the perfect time.

Shiny: A ripe watermelon will not be shiny, so avoid any that are. By following these guidelines, you can select a ripe and sweet watermelon every time.

Based on the guidelines, which one is the ripe and sweet melon? Also show me the coordinates of the things that you mention.

The ripe and sweet melon <114,453,227,595> would be the one with a dark and dull exterior, an orange field spot, and larger webbing.

Which place should I go to if I want to buy lemons?

Fruits and Vegetables

Ok. Is this the correct place?

No, you are in the fresh meat area. The correct place to buy lemons is in the Vegetables department as shown in the supermarket image.

Okay, here is the place. Can you help me find the lemons? Also show me the coordinates of the things that you mention.

Sure! The lemons <236,218,646,448> are located in the middle of the image, nestled between the tomatoes and the peppers.

A.13.4 MULTI-IMAGE REASONING

In which of these situations can I drive on ahead?

In the second image, you can drive on ahead because the traffic light is green.

What is the bike experiencing in image 1? Which one fits best, image 2 or image 3, and why?

The bike in image 1 is experiencing rust and wear, as indicated by the rusted metal parts and the bent handlebars. Image 2, with its focus on the bicycle wheel, fits best as it provides a close-up view of the bike's wheel, which is the part most directly related to the bike's condition.

I have these ingredients in my fridge. What can I make using all of these? Explain.

You can make a banana bread using all of these ingredients. The ripe bananas from image 3 can be mashed and combined with the flour from image 1 and the eggs from image 4 to create a moist and flavorful banana bread. The chocolate chips from image 2 can be mixed into the batter for added texture and sweetness.

A.13.5 UI UNDERSTANDING

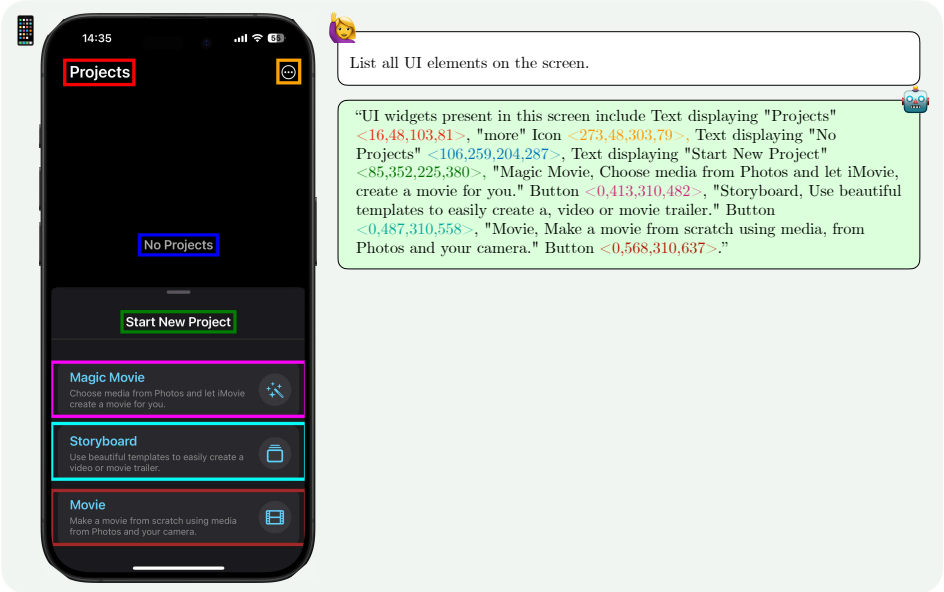

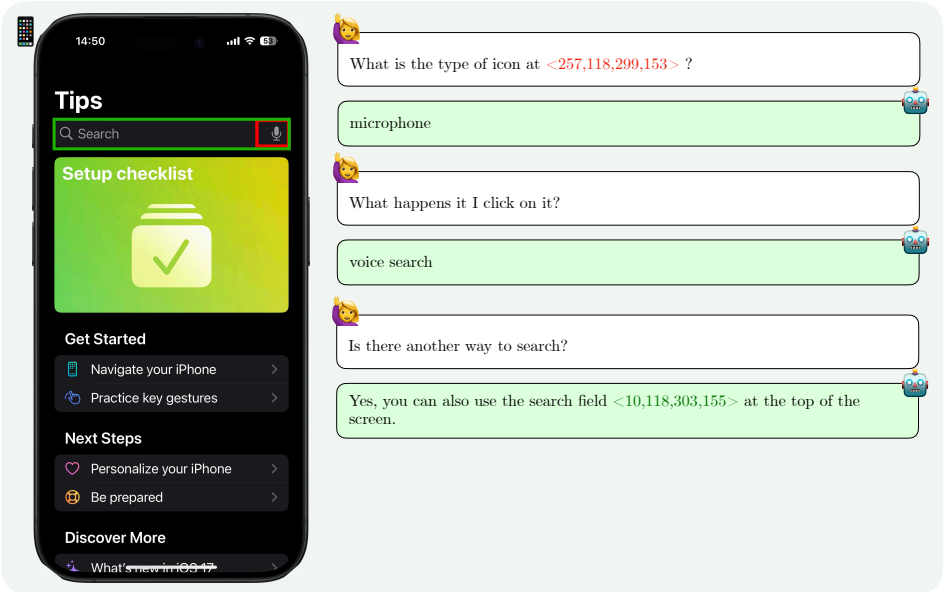

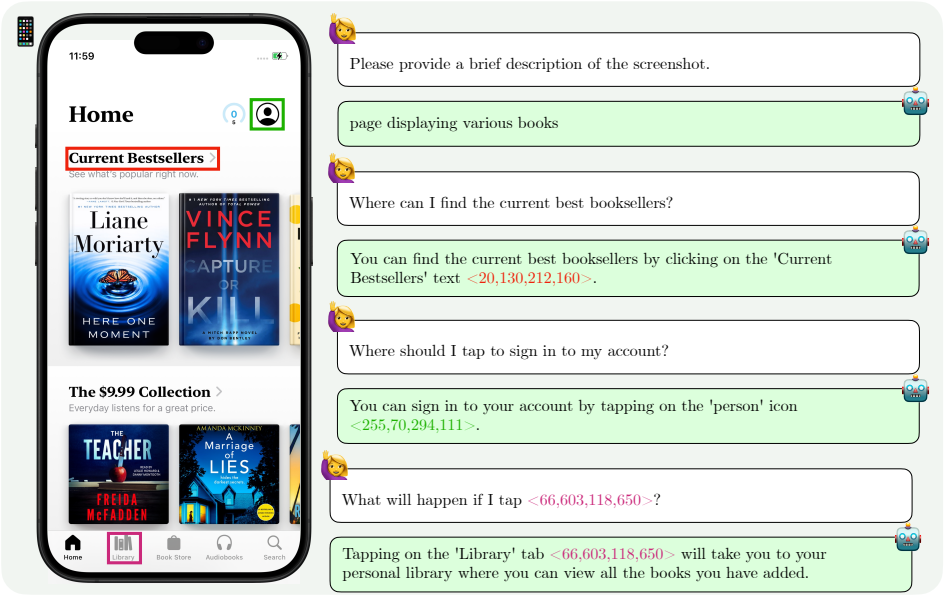
11:59
Home
Current Bestsellers
See what's popular right now.
Liane Moriarty
HERE ONE MOMENT
VINCE FLYNN
CAPTURE OR KILL
The $9.99 Collection
Everyday listens for a great price.
THE TEACHER
FREIDA McFADDEN
AMANDA MCKINNEY
A Marriage of LIES
Home
Library
Book Store
Audiobooks
Search
Please provide a brief description of the screenshot.
page displaying various books
Where can I find the current best booksellers?
You can find the current best booksellers by clicking on the 'Current Bestsellers' text <20,130,212,160>.
Where should I tap to sign in to my account?
You can sign in to your account by tapping on the 'person' icon <255,70,294,111>.
What will happen if I tap <66,603,118,650>?
Tapping on the 'Library' tab <66,603,118,650> will take you to your personal library where you can view all the books you have added.